FINITE ELEMENT ANALYSIS OF MULTI-DISK ROTOR-BEARING SYSTEM WITH TRANSVERSE CRACK

A THESIS SUBMITTED IN PARTIAL FULFILLMENT
OF THE REQUIREMENTS FOR THE DEGREE OF

Master of Technology (Research)

in

Mechanical Engineering

by

Bala Murugan S

Roll No: 612ME310

Department of Mechanical Engineering

National Institute of Technology

Rourkela - 769008

March 2015

FINITE ELEMENT ANALYSIS OF MULTI-DISK ROTOR-BEARING SYSTEM WITH TRANSVERSE CRACK

A THESIS SUBMITTED IN PARTIAL FULFILLMENT
OF THE REQUIREMENTS FOR THE DEGREE OF

Master of Technology (Research)

in

Mechanical Engineering

by

Bala Murugan S

Roll No: 612ME310

Under the Guidance of

Dr. R.K. Behera

Department of Mechanical Engineering

National Institute of Technology

Rourkela - 769008

Declaration

I hereby declare that this submission is my own work and that, to the best of my knowledge and belief, it contains no material previously published or written by another person nor material which to a substantial extent has been accepted for the award of any other degree or diploma of the university or other institute of higher learning, except where due acknowledgement has been made in the text.

(Bala Murugan S)

Dr. Rabindra Kumar Behera
Department of Mechanical Engineering
National Institute of Technology
Rourkela 769008
Odisha, India.

National Institute of Technology Rourkela

Email:
rkbehera@nitrkl.ac.in
rabi57@rediffmail.com
Phone:
+91-661-246-2504 **(O)**
+91-661-246-3504 **(R)**
+91 8895444886 **(M)**

Certificate

This is to certify that the thesis entitled, "Finite Element Analysis of Multi-Disk Rotor-bearing System with Transverse Crack" being submitted by Shri Bala Murugan S is a bona fide research carried out by him under my supervision in partial fulfilment of the requirements for the Degree of Master of Technology (Research) in Machine Design and Analysis at Mechanical Engineering Department, National Institute of Technology, Rourkela.

To the best of my knowledge, the matter embodied in the thesis has not been submitted to any other University / Institute for the award of any Degree or Diploma. The matter embodied in this thesis is original and has not been used for the award of any other degree.

I wish him all success in his future endeavour.

Dr. R.K. Behera (Supervisor)
Associate Professor
Department of Mechanical Engineering
National Institute of Technology
Rourkela- 769 008

Acknowledgements

With deep regards and profound respect, I avail this opportunity to express my deep sense of gratitude and obligation to Prof. Rabindra Kumar Behera, Associate Professor, Department of Mechanical Engineering whose valuable suggestions, interests, patience and inspiring guidance, constructive criticism throughout in this research work which made this work a truly rewarding experience by several altitudes.

I am sincerely thankful to Prof. S.S. Mohapatra, Head, Department of Mechanical Engineering, for his advice and providing necessary facility to carry this work.

I would like to thank Prof. S.K. Panda, Department of Mechanical Engineering, for his advice and providing necessary suggestions to make forward this work.

I would also like to thank Prof. S. K. Sahu, Department of Civil Engineering, NIT Rourkela, and Prof. Md. Equeenuddin, Department of Mining Engineering for their talented advices.

I am also thankful to my friends and colleagues for standing by me during the past difficult times. Particularly, I am indebted to Mr. Alok Ranjan Biswal and Mr. Sudhansu Meher for their utterly selfless help.

I am greatly indebted to my grandfather Palaveasam Assary, Mother S. Velammal, Father P. Subiramaniyan and Sister S. Amirthavalli for their loving support throughout. Finally I am thankful to all my other family members and friends for their support in completion of the present dissertation.

Bala Murugan S

Table of Contents

Abstract

The vibration analysis of rotating systems is pronounced as a key function in all the fields of engineering. The behavior of the rotor systems are mainly resulting from the excitations from its rotating elements. There are several numerical methods present to analyze the rotor-bearing systems. Finite element method is a key tool for dynamic analysis of rotor bearing system. The current study describes a multi disk, variable cross section rotor-bearing system with transverse crack on axisymmetric elements supported on bearings in a fixed frame. The shaft in the rotor-bearing system is assumed to obey Euler-Bernoulli beam theory. The equation of motion of the rotor-bearing system is derived by Lagrangian approach along with finite element method. Finite element model is used for vibration analysis by including rotary inertia and gyroscopic moments with consistent matrix approach. The rotor bearing system consists of two bearings and two rigid disks. One disk is overhung and the other one is placed between the bearings. Internal damping of the shaft and linear stiffness parameter of the bearings are taken into account to obtain the response of the rotor-bearing system. The rotor has variable cross-section throughout the configuration. The disks are modeled as rigid and have mass unbalance forces. The critical speed, unbalance response and natural whirls are analyzed for the typical rotor-bearing system with transverse crack. Analysis includes the effect of crack depths, crack location and spin speed. The results are compared with the results obtained from finite element analysis. The bearing configurations are undamped isotropic and orthotropic. The natural whirl speeds are analyzed for the synchronous whirl for both the uncracked and cracked rotor bearing system using Campbell diagrams. The effect of transverse crack over the starting point of the system instability regions in the rotating speed axis with zero asymmetric angle is examined. Further, Houbolt's time integration scheme is used to obtain the phase diagrams and frequency response for both the bearing cases to study the stability threshold. Analyses are carried out by using numerical computing software.

Keywords: *Finite Element Method, Rigid disk, Transverse crack, Unbalance response, Whirl speeds.*

List of Tables

List of Figures

Sl. No.	Figure caption	Page No.

Sl. No.	Figure caption	Page No.

Sl. No.	Figure caption	Page No.

Nomenclature

A_1	Overall cracked element cross-sectional area
$\mathrm{C_{ij}}$	Bearing damping coefficient, i, j = *V, W*
$[C]$	Bearing damping matrix
E	Young's modulus of the shaft material
e	Centroid location of A_1 in y-axis
$[G^e]$	Element gyroscopic matrix
h	crack depth in the radial direction
I	Second moment of inertia of the shaft
I_i	Constant quantities during the rotation of the cracked shaft, i = 1, 2
$[I]$	Identity matrix
$I_{\bar{X}}(\mathrm{t})$	time-varying area moments of inertia of the cracked element about X axis
$I_{\bar{Y}}(\mathrm{t})$	time-varying area moments of inertia of the cracked element about Y axis
I_X	Area moments of inertia of the overall cross sectional area of the cracked element about (A_1) X axis
I_Y	Area moments of inertia of the overall cross sectional area of the cracked element about (A_1) Y axis
$\mathcal{I}_D$, $\mathcal{I}_P$	Diameter and polar mass moments of inertia of the shaft per unit length
$\mathcal{J}^e$	Kinetic energy of the element
$[K]$	Stiffness matrix
$\mathrm{k_{oc}(t)}$	Time varying stiffness matrix of the open cracked element
$\mathrm{k_{o1}}$, $\mathrm{k_{o2}}$	secondary stiffness matrices due to the open crack
k_{ij}	Bearing stiffness coefficient, *i, j = V, W*
l	Length of the shaft element in the finite element model
$[M]$	Mass matrix

m_d	Disk mass
$N_i(s)$	One dimensional quadratic Lagrangian shape function
N_i	Translational shape function, i = 1, 2, 3, 4
N_i'	Rotational shape function, i = 1, 2, 3, 4
$\mathcal{P}^e$	Potential energy of the element
$\{q^e\}$	Nodal displacement vector
$\{q_c\}$	Unbalance response associated with cos (Ωt)
$\{q_s\}$	Unbalance response associated with sin (Ωt^2)
R	shaft radius
s	axial distance within an element
T	Kinetic energy of the disc
T_S	Total kinetic energy of the system
t	time
U_S	Total potential energy of the system
(V, W)	Translational displacements in Y and Z directions
X Y Z	fixed reference frame
$\{Q^e\}$	External force vector relative to fixed reference frame
$\{Q_c^e\}$	Unbalance force respect to cos (Ωt)
$\{Q_s^e\}$	Unbalance force respect to sin (Ωt^2)

Greek

$[\Psi]$	Matrix of translational displacement functions
$[\Phi]$	Matrix of rotational displacement functions
ϕ	angle between the major axes of the crack and the shaft
ε	spin angle

Ω	spin speed $= \dot{\varepsilon}$
ω	whirl speed
μ	Element mass per unit length
μ	Non-dimensional crack depth
η_H	Hysteretic damping coefficient of the shaft material
η_V	Viscous damping coefficient of the shaft material
(θ, ζ)	Small angle rotations about Y and Z axes
λ	whirl ratio
γ	Proportional damping coefficient

Superscripts

T	Transpose
$\cdot$	Dot, differentiation with respect to time
$'$	prime, differentiation with respect to axial distance s
d, e, b, s	refers to disk, element, bearing, and system
j	cracked element

Subscripts

T, R, B	refers to translational, rotational and bending

Chapter-1

Introduction

The subject rotor dynamics is called an idiosyncratic branch of applied mechanics which deals with the performance and detection of spinning structures. The predictions of the system dynamic aspect are meticulously essential in the design of rotating structures. Generally it analyzes the behaviour of rotating structures which ranges from fans, gear trains to turbines and aircraft jet engines. Rotating systems generally develop instabilities which are excited by unbalance and the internal makeup of the rotor system and must be corrected. This is the prime area of interest for the design engineers who model the rotating systems.

1.1. Background and Significance

From ISO definition, rotor can be defined as a body which is suspended through a set of cylindrical rest or bearings that grants the system to rotate freely about an axis secured in space. In the basic level of rotor dynamics, it is related with one or more mechanical structures (rotors) supported by bearings that rotate around a unique axis. The non spinning structure is called a stator. When the spin speed increases the amplitude of vibration increases and is maximum at a speed called critical speed. This amplitude is often elevated by unbalance forces from disk of the spinning system. When the system reaches excessive amplitude of vibration at the critical speed, catastrophic failure occurs. Normally turbo

machineries frequently develop instabilities which are mainly due to the internal configuration, and should be rectified.

Often rotating structures originates vibrations depending upon the complexity of the mechanism involved in the process. Even a small misalignment in the machine can increase or excite the vibration signatures. System vibration behaviour due to imbalance is the main aspects of rotating machinery, and it must be measured in detail and reviewed while designing. Every object including rotating structures shows natural frequency depending on the complexity of the structure. The critical speed of these rotating structures arises when the rotational speed meets with its natural frequency. The first critical speed can be encountered at the lowest speed. However as the speed increases further critical speeds can also be spotted. It is very essential to reduce the rotational unbalance and excessive external forces to minimize the overall forces which actuate resonance. The major concern of designing a rotating machine is, avoiding the vibration in resonance which creates a destructive energy. Situations involving rotation of shaft near critical speed must be avoided. When these aspects are ignored it might results in wear and tear of the equipment, failure of the machinery, human injury and sometime cost of lives.

1.2. Basic principles

To model the actual dynamics of the machine theoretically is a cumbersome task. Based on the simplified models, the calculations are made to simulate various structural components. The dynamic system of equations have interesting feature, in which the off-diagonal elements are stiffness, damping, and mass. These three elements can be called as, cross-coupled stiffness, cross-coupled damping, and cross-coupled mass. Although there is a positive cross-coupled stiffness, a deflection will originate a reaction force opposite to the direction of deflection, and also the reaction force can be in the direction of positive whirl.

When these forces are large compared to the direct damping and stiffness, the rotor will be unstable. If a rotor is unstable it typically needs a prompt shutdown of the machine to avoid breakdown.

1.3. History of Rotor Dynamics

Rotor dynamics has been steered further by its practice than by its theory. This remark is particularly related to the initial history of rotor dynamics. History and research on rotor dynamics spells at least 14 decades.

1.3.1. From Rankine to Jeffcott Rotor systems

The history of rotordynamics begins with W. J. M. Rankine [1], who first performed an analysis of a rotating shaft (Figure 1.1a) in 1869. He concludes that beyond a certain spin speed, the shaft is appreciably bent and whirls around the bent axis. He illustrates that, this speed as the whirling speed of the spinning shaft.

a. b.

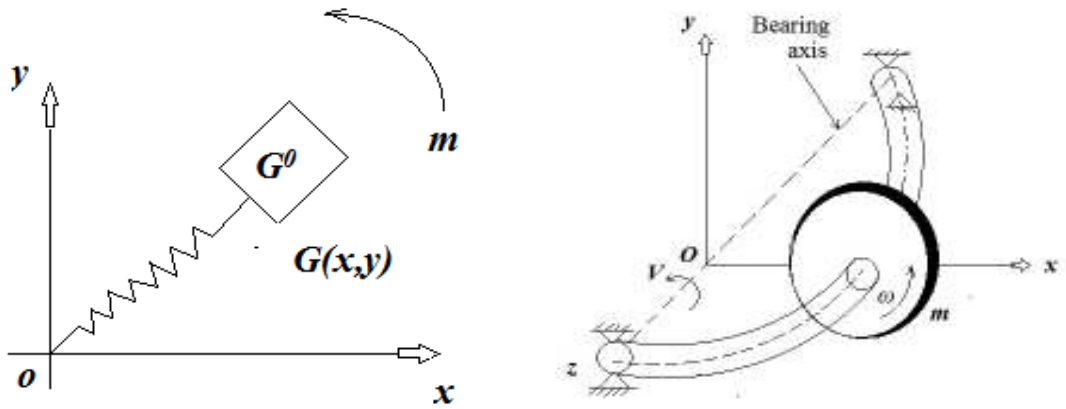

Figure 1.1 Rotor model (a) Rankine model (b) Jeffcott rotor model

Whirling of the shaft refers to the shift of the disk's centre of mass in the deflected position from a plane perpendicular to the bearing axis. Whirl frequency '*v*' mainly depends on the stiffness and damping of the rotor and the amplitude becomes a function of

the frequency ω, (excitation force) and magnitude. Critical speed , ω_{cr}, of the system exists when the excitation frequency coincides with a natural frequency, ω_{nf}, and this can lead to the enormous vibration amplitudes.

De Laval [1] (Swedish Engineer) in 1883 succeeds with a single-stage steam impulse turbine for marine applications which operates at 0-42000 rpm. He first decided to use a rigid rotor, but later he came with a flexible rotor and unveils that it was feasible to operate above the critical speed by operating at a spin speed closely about seven times the critical speed. A flexible shaft of negligible mass with a rigid disc at its midspan is called as a Jeffcott [1] rotor (Figure 1.1b). The fundamental theory of rotor dynamics first recorded which can be found in a masterly article of Jeffcott in 1919. However Jeffcott confirmed Föppl's [1] prediction that a stable supercritical solution occurs and decided to continue with Föppl's study. Föppl used an undamped model to show that an unbalanced disc would whirl synchronously with the heavy side flying out when the rotation is subcritical and with the heavy side flying in when the rotation is supercritical

1.4. Research Goals and Analysis Approach

By the beginning of the twentieth century, the developments in the field of rotor dynamics was summarised in the classic book written by Stodola [1] in 1924. Then turbine manufacturers around the world started to design, analyze and operate rotors at super critical level. On the contrary Rankine's model neglects the Coriolis [1] acceleration and states that the system cannot be stable if it operated over the critical speed.

The proposed research study aims to find out the behaviour of the dynamic rotor-bearing system supported on two rolling element bearings. There have been much investigations related to the field of rotordynamics during the past few decades. By looking in to all the previous published works, the part of literatures on rotor dynamics is most

concerned with diagnosis of imbalance response, critical speeds, natural whirl frequencies and instability analysis. The presence of transverse crack on the rotor has been a keen attention for researchers. Presence of crack in the rotating systems will lead to the time-varying stiffness (parametric inertia) and causes instability and gives severe vibration signatures under specified operating limits. Few researchers speculated on the opportunity of Rotor Internal Damping (RID) or Material Damping (MD).

The following analyses are carried out for the current research work;

1. Dynamic analysis of an undamped rotor-bearing system without transverse crack.
2. Dynamic analysis of a damped rotor-bearing system without transverse crack.
3. Dynamic analysis of an undamped rotor-bearing system with transverse crack

All the above three analyses are carried out for two bearing cases; case (a) isotropic and case (b) orthotropic for the speed range of 0-30000 rpm. Finite element method is used to model the rotor-bearing system by incorporating internal damping with crack. By using Lagrangian formulation the equation of motion is developed for the discrete elements and shaft. The effect of transverse crack is studied over its stability region in the spin speed axis. From the finite element stiffness matrix of the cracked element, it is observed that, the cracked element stiffness matrix has time-periodic components with the frequency of 2Ω. The analysis is presented in detail for the uncracked and cracked rotor-bearing system in subsequent chapters.

The shaft is modelled as Euler-Bernoulli beam incorporating translational inertia, rotary inertia, bending deformation, gyroscopic effects and internal damping. Natural frequencies of the cracked rotor-bearing system also carried out. The results obtained for the dynamic analysis of the uncracked rotor-bearing system by using numerical analysis.

Chapter-2

Literature Review

2.1. Introduction

The dynamic analysis of high-speed rotating machinery on rolling element bearings has been always a challenging task. The most interesting part is the design of rotating machineries. In general all the spinning structures show vibration signatures and need frequent analysis to stretch their performances. The rotating machines have great engineering applications when it's come to industries. Accurate analysis and prediction of dynamic characteristics is prime objective in the design of rotating structures.

2.2. Dynamic analysis of rotor-bearing systems

There have been several investigations related to the topic of rotor dynamics for the past few decades. The flexible rotor-bearing systems have been analyzed with many mathematical methods. The use of finite element methods in the dynamic analysis of rotor-bearing systems provides better results. Several researchers have done their extensive investigations on the spinning rotors since the last four decades. Here some of the literatures were studied for their contribution on the field of rotor dynamics that concerns with prediction of critical speeds, mass imbalance, natural whirl frequencies and stability thresholds.

The author mainly discussed about the basic concepts and methods of rotordynamic systems. The analysis of various types of rotors are discussed and presented by Genta [1].

An important modelling and analysis method to obtain exact solutions for multi-stepped rotor-bearing systems with distributed parameters was carried out by Hong and Park [2]. In first example the system was compared with FEM model for validation. In second example a parametric study was carried out for two shafts with different lengths and diameters. In the final example, an unbalance response analysis was performed to show the applicability of the proposed method.

A new method was introduced by Joshi and Dange [3] for calculating the critical speeds of a general flexible rotor supported on flexible or rigid bearings which includes the effect of distributed mass and inertia of the shaft along with the transverse shear effect. Bearing mass, damping, coupling flexibilities and external loads are also considered to find the effect of coupling flexibilities in critical speeds.

Modal analysis for continuous rotor systems with various boundary conditions was presented by Lee and Jei [4]. The mode shapes, backward and forward whirl speeds of a rotating shaft are presented as spin speed and boundary conditions vary. Boundary conditions with the effects of asymmetry on the system dynamic characteristics are investigated by them.

Rao et al. [5] used the finite element technique to obtain the eigenvalue and stability analysis of rotors by considering the distributed bearing stiffness and damping. Two models with uniform and parabolic distribution were analyzed. The stability limits were studied for rotor supported on cylindrical, tilting pad and offset and three lobe journal bearings.

A method of dynamic reduction procedure which does not require either sub structuring or lumping was performed by Kim and Lee [6]. The method of modal transformation was derived from the isotropic undamped static part of the rotor equation, and a comprehensive study of the effects of varying the number of retained modes and the bearing properties was elaborated.

Zhao et al. [7] have established for symmetrical single-disk flexible rotor-bearing system. The motions of journal and disk have been simulated with fourth-rank Runge-Kutta method. Non-linear transient simulation and unbalanced responses are also investigated.

Shih and Lee [8] presented a new method for estimating unbalance distributions of flexible shafts and constant eccentricities of rigid disks based on the transfer matrix method for analyzing the steady-state responses.

Tiwari and Chakravarthy [9] used an identification algorithm based estimation of unbalances and dynamic parameters of bearings by using impulse response measurements for flexible rotor–bearing systems. The identification algorithm has been tested with the measured noise in the simulated response.

The effects of bearing support flexibility on the rotor dynamic analysis for the first forward and a backward critical speed was studied numerically and experimentally by Sinou et al. [10]. They discussed the measured FRF for various rotational speeds, eigenfrequencies and the associated Campbell diagram from the numerical model and the experimental results.

The dynamic modeling of rotor-bearing system with rigid disks and discrete bearings were analyzed with finite element method by Nelson and Mc Vaugh [11].

The effect of rotatory inertia, gyroscopic moments, axial load and internal damping was included by Nelson [12]. He has not included the shear deformation or axial torque in the observation. He generalizes the present study with his previous published paper by utilizing the Timoshenko beam theory for obtaining the shape functions. He has compared the results obtained from FEA with the classical Timoshenko beam theory (closed form) for both the rotating and nonrotating shaft systems.

The analysis of Jeffcott rotor-bearing model is presented by Greenhill and Cornejo [13] to predict the critical speed produced by the unbalance excitation of a backward resonance mode. Prediction of the critical speed was given with the test data. Their study shows that the resonance occurs due to the backward mode with the recommendation to avoid the unique critical speed situation.

Nandi and Neogy [14] studied the stability analysis of asymmetric rotors in a rotating frame using finite element method. It shows the efficiency of their method which indicates that, only the non-zero terms and their respective rows and columns positions of all the related matrices can be stored and carried forward for the analysis.

The non-linear dynamic analysis of a horizontal rigid rotor with unbalance is studied by Tiwari et al. [15]. The concept of higher order Poincare map and interpolation technique were applied to find out the fixed point and stability of the system.

To identify the fault in a rotor bearing system, Sudhakar and Sekhar [16] used the equivalent load minimization method. Two approaches namely equivalent loads minimization and vibration minimization method are used to identify the fault. Finally the unbalance fault was identified for only one location by measuring transverse vibrations.

Bachschmid et al. [17] presented a model-based method for multiple faults identification. They had done this by least-square fitting approach in the frequency domain. To validate the identification procedure they presented numerical applications for two parallel faults and some experimental results which are obtained on a test-rig.

A method proposed by Sinha et al. [18] is to estimate the rotor unbalance and misalignment from a single machine run-down. From the identification they assumed that, the source of misalignment is at the couplings of the multi-rotor system. Finally they demonstrated the method by using experimental data from a machine with two bearings.

Arun and Mohanty [19] described a model based method to analyze the rotor–bearing system with misalignment and unbalance. The experimental results were obtained by the residual generation technique. They also obtained the residual forces due to presence of faults. Finally with the help of this model based technique, the condition of fault and the fault locations were identified.

Vania and Pennacchi [20] suggested a model-based diagnostic technique that can be used for the rotor health analysis. To identify the faults in rotating machines they developed a method to measure the accuracy of the results that are obtained with model-based techniques. By using both the machines responses simulated with mathematical models and experimental data on a real machine, the authors tested the capabilities of these methods.

By representing the equivalent force system, the effect of the faults is modelled by Pennacchi et al. [21]. The model is fully assembled by the sub models of the rotor discrete elements like bearings and foundation. Some identification techniques such as the least squares identification are used in frequency domain to increase the accuracy.

Lees et al. [22] overviewed the recent evaluation in the field of rotor dynamics which has a significant practical importance. The models assists the complex turbo-machinery monitoring which includes rotor balancing, rotor bow, rotor misalignment, rotor crack and bearing parameter estimations.

The goal of Isermann [23] is to generate the several symptoms indicating the difference between nominal and faulty status in the model-based fault detection. He determined the faults by applying inference methods based on the different symptoms in the fault diagnosis procedures.

Complete theoretical models of a motor-flexible coupling-rotor system was given by Xu and Marangoni [24]-[25] to understand the dynamic characteristics of the faults such as, shaft misalignment and rotor unbalance. They derived the equation of motion from component mode synthesis method and conducted an experimental study to verify the theoretical results with a simple flexible coupling and a helical coupling.

Forced response of undamped rotating shaft with distributed parameter are analysed by Lee et al. [26] by using modal analysis technique. The analysis includes various boundary conditions to analyze the undamped gyroscopic systems with Galerkin's method for the forced response. Numerical examples for both the methods are illustrated and the results are compared and discussed by them.

The study of a misaligned rotor-ball bearing systems driven by a flexible coupling is done by Lee et al. [27]. They carried out the experiments extensively to distinguish the difference between experimental and theoretical results. From their observation, they found that the natural frequency of the misaligned rotor system increases largely with the misalignment direction.

Sakata et al. [28] carried out finite element analysis of a lightweight rotor system, which has discrete elements like flexible disk with flexible blades and a flexible shaft with rigid bearings. In order to reduce the dimension of matrices, they considered the shaft and blades as beam elements, and the disk as annular elements. They conducted the test on a model rotor to compare the results with the experimental data.

Khulief and Mohiuddin [29] developed a dynamic rotor-bearing system by using finite element method. Their model includes the gyroscopic moments and anisotropic bearings. They obtained the reduced order model by using modal truncation for dynamic response analysis and presented with two types of modal truncations; (i) with planar (undamped) modes and (ii) with complex (damped) modes.

A finite element model is presented by Ku [30] to study the whirl speeds and stability of the rotor-bearing systems. He combined the effects of transverse shear deformations; internal viscous dampings and hysteretic dampings in the formulation in addition to the effects of translational and rotatory inertia and the gyroscopic moments. He compared the results of whirl speeds and damped stability analysis with other previously published works.

The dynamic stability of a rotating shaft is studied by Chen and Ku [31] with finite element method. Bolotin's method is used to obtain the dynamic instability diagrams for the various rotating speeds for Timoshenko beam. They conclude that the sizes of these regions increases as the spin speed of the system increases.

Flexible rotor having unbalance, and supported by ball bearings was studied by Villa et al. [32] for non-linear dynamic analysis. The bearings are modelled as two degree of freedom system by considering the kinematics of the rolling elements. They analyzed

the system stability in the frequency-domain by using a perturbation method which is applied to known harmonic solutions in time domain.

Finite element model of Timoshenko beam supported on hydrodynamic bearings including internal damping were studied by Kalita and Kakoty [33]. By using Campbell diagrams they calculated the critical speeds for synchronous whirl in different operating conditions. They observed that in addition to the natural whirl frequencies, another whirling frequency appears for every spin speed, and they also found that, this happens when the spin speed is half.

The study of the flexural dynamic behaviour of a general rotating system, based on the use of complex co-ordinates and finite element method is elaborated by Genta [34]. The study includes the non-rotating parts of the machine and two types of dampings, namely viscous and hysteretic.

Thomas et al. [35] presented the formulations of three degrees of freedom system at each of two nodes of Timoshenko beam theory. They studied the convergence rates and compared with the calculated natural frequencies of two cantilever beams.

A complex rotor-bearing-support system was taken for the general analysis by Adams [36]. Proper handling of various non-linear effects is a main feature of his analysis. The study presents the developments of the analysis, comparison with experiment study and examples and its use in the industrial applications.

A finite element model of non-axisymmetric rotors on non-isotropic spring support in a rotating frame is presented by Nandi [37]. In his work he shows that the proposed reduction technique works well for a rotor supported on non-isotropic (orthotropic) springs.

Murphy and Vance [38] describe the modelling procedures for the rotor-bearing systems which includes the effects of damping, gyroscopic effects. In addition to the characteristic polynomial, stability prediction and critical speeds are also estimated with good accuracy without missing any modes.

Lee and Choi [39] proposed an optimum design approach to show the speed and load dependent stiffness effect on the system dynamic behaviour to demonstrate the effectiveness of a multi-stepped rotor-bearing system supported on two angular contact ball bearings. Transfer matrix method is used to obtain eigenvalue of the system and as an optimization technique the augmented Lagrange multiplier (ALM) method is used. From the results, they show the effect of stiffness on the system dynamic behaviour.

Dynamic behaviour of a complex flexible rotor-bearing system is studied by Wenhui et al. [40]. The unsteady oil-film force model was described by three functions. In addition to that the bifurcation and chaos behaviours were found by calculating the maximum Lyapunov exponent of the system. They carried the experimental analysis to compare the calculated results.

Patel and Darpe [41] studied the use of forward or backward whirl (full spectra), and showed the possibility of misalignment. The information yields an important tool to unconnected faults that generate the same frequency spectra (e.g. crack and misalignment) and lead to a more definite misalignment diagnosis. Finally full spectra and orbit plots were efficiently used to reveal the unique nature of misalignments.

Zorzi and Nelson [42] analyzed rotor system with internal damping. The model consisted of viscous as well as hysteretic damping. It is shown that the material damping in the rotor shaft introduces rotary dissipative forces.

Rao [43] explained the theory of computational aspects and applications of vibrations in a simple manner with computational techniques.

Papadopoulos [44] presented the theory of strain energy release rate combined with linear fracture mechanics approach to study rotating shafts with cracks. The main goal of his research is to give the engineer an early identification of the crack in the rotor.

Chasalevris and Papadopoulos [45] investigated a stationary shaft with two cracks with coupled bending vibrations. They used Euler–Bernoulli beam theory to define the equations for natural frequencies and coupled response of the shaft. Their study focused on the horizontal and vertical planes of a cracked shaft. Finally they presented the experimental analysis for coupled response and eigen frequencies measurements of the corresponding planes.

Dimarogonas and Papadopoulos [46] investigated an open cracked de Lava1 rotor with dissimilar moments of inertia. Furthermore, under the assumption of large static deflections, the analytical solutions are obtained for the closing crack. They found the local flexibility function by experiments and a solution is developed for the same.

Shudeifat et al. [47] investigated the effect of crack depth and verified with experiments through a general harmonic balance technique of a rotor-bearing-disk system. They considered the breathing and open crack models in their analysis. FEM and general harmonic balance solutions were derived for the two types of cracks which are valid for damped and undamped rotor systems.

Chen et al. [48] studied a cracked rotor system with asymmetrical viscoelastic supports to develop nonlinear governing equations of motion. The effects of crack and other system parameters on the dynamic stability of spinning rotor system were also investigated by them.

Darpe et al. [49] studied a simple Jeffcott rotor with two transverse cracks. The effect of two cracks on the breathing mechanism and unbalance response of the rotor

system were also studied by them. They studied in detail, the effect of orientation of the breathing crack with respect to open crack on the dynamic response.

Fu et al. [50] studied a rotating shaft with a transverse crack for the nonlinear dynamic stability. They constructed the deflections of the system with a crack by using the equivalent line-spring model. They found the unstable regions using Runge–Kutta method and Floquet theory. The effects of crack depth, crack position, disk position, disk thickness and spinning speed on the principal unstable regions were also discussed by them.

Gasch [51] - [52] provided a comprehensive analysis for a cracked rotor system to predict its stability behaviour and forced vibrations due to unbalance of the crack and the disk. He mentioned that his study is restricted to the Laval rotor and established the early crack detection on the rotor.

Sekhar [53] studied the finite element analysis of a rotor system for the flexural vibrations by including two transverse open cracks. His study also carries the eigenvalue analysis and stability study of the system including two open cracks. The eigenfrequencies are calculated for the influence of one crack over the other and the mode shapes for the threshold speed limits.

Sekhar and Dey [54] focused on the stability threshold of a rotor-bearing system having a transverse crack by using finite element method, considering various crack parameters, shaft internal damping (viscous and hysteretic) and geometric parameters. They showed that the instability speed has reduced considerably with increase in crack depth and influenced more with hysteretic damping compared to viscous damping.

Sekhar [55] summarized different kinds of application on double/multi-cracks to note the influences and identification methods in vibration structures such as beams, rotors, pipes, etc. He brings out the multiple cracks effect and their identification by the state of his research.

Sinou [56] analyzed a rotor system for its stability with a transverse breathing crack by considering the effects of crack depth, crack location and the shaft's spin speed. The harmonic balance method used by him is to calculate the periodic response of a non-linear cracked rotor system. He also investigated the system for the effects of some other system parameters on the dynamic stability of non-linear periodic response.

The free vibrational analysis of a multi-cracked rotor is studied by Tasi and Wang [57]. The cracks are assumed to be in the first mode of fracture, i.e. the opening mode. Based on the Timoshenko beam theory, the frequency equations are constructed and assembled with each segment of the multi-step and multi-cracked rotor. The effects of both relative distances of cracks are taken into account for free vibration analysis.

A boundary tracing method is given by Turhan [58] for the construction of stability charts for non-canonical parametrically excited systems. This method is used as an extension to cover the combination resonances of the well known Bolotin's method. The proposed method reduces the boundary tracing problem into an eigenvalue analysis problem of some special matrices.

Darpe et al. [59] studied a rotating cracked shaft for the coupling between longitudinal, lateral and torsional vibrations. The elemental stiffness matrix of a Timoshenko beam got modified due to presence of crack. Two analyses were included in their study (i) coupled torsional–longitudinal vibrations and (ii) coupled torsional–bending vibrations with a breathing crack model.

A rotating shaft is analysed for the influences of transverse cracks by Sinou and Lees [60]. Two main issues such as the changes in modal properties and the influence of breathing cracks on dynamic response are addressed by them. The resulting orbits during transient operations of a cracked rotor are also examined by the authors.

A simple rotor with a breathing crack is studied by Jun et al. [61]. The equations of motion and the breathing crack model is further simplified to a switching crack model. The conditions for crack opening and closings are derived by using the switching crack model for crack identification. They observed that the vibration characteristics of a cracked rotor can be identified from the second horizontal harmonic components measured near to the second harmonic resonant speed.

Finite element analyses of a rotor-bearing system having a slant crack were studied for flexural vibrations by Sekhar and Prasad [62]. A developed flexibility matrix and stiffness matrix of a slant crack are used in the analysis subsequently to find frequency spectrum and steady state response of the cracked rotor.

A model based method was proposed by Sekhar [63] for the on-line identification of cracks in a rotor. He accounted the equivalent loads and fault-induced to the system in his mathematical model. Identification of the cracks are carried for their depths and locations on the shaft. Finally the nature and the symptoms of faults are found by fast Fourier transform analysis.

Online identification of malfunctions in the rotor systems was discussed by Jain and Kundra [64] with a model based technique. The fault model of the system is referred for study by the mathematical representation of equivalent load. Identification of unbalance response is validated with basic principle of the technique, through numerical simulations as well as by experiments.

A rotating shaft with a breathing crack was studied by Georgantzinos and Anifantis [65]. They considered the cracked area with the effect of friction and by applying the energy principles a portions of crack surfaces were found. The direct and the cross-coupled flexibility coefficients were also determined by them.

A new method was proposed by Binici [66] to obtain the eigenfrequencies and mode shapes of beams for multiple cracks which are subjected to axial force. The effects of crack and axial force levels on the eigenfrequencies of the beam were studied. He considered two cases in his analysis (i) simply supported and (ii) cantilever beam. During the investigation the author found that the eigenfrequencies are strongly affected by crack locations. The conclusion from his study shows that, the proposed method can be used to predict the critical load for damaged structures.

Non-linear behaviour of a rotor with a breathing crack was analysed by Sinou [67]. The relative orientation between the cracks and the unbalance of the rotor system were studied. The study indicates the emerging of super-harmonic frequency components which provides useful information on the presence of cracks.

A Jeffcott rotor with a crack was studied for critical speed and sub harmonic resonances by Darpe et al. [68]. The study includes three crack models; (i) breathing crack, (ii) switching crack and (iii) open crack. The experimental investigations were performed for the peak response variations and change in orbit orientation. Their experimental investigation shows that, the orbit orientation changes through the sub harmonic resonances.

A rotating shaft with an open transverse surface crack was investigated for the coupling of longitudinal and bending vibrations by Papadopoulos and Dimarogonas [69]. The effects of unbalance and gravity are also included in their study.

Vibration and stability analysis of cracked hollow-sectional beams were carried by Zheng and Fan [70]. Their analysis includes influences of sectional cracks and deeper penetration on the stability of the beam. Hamilton's principle is used by them to derive the governing equations.

Hwang and Kim [71] developed a method to detect the damages of structures by using frequency response function. The method uses only a subset of vectors from the full set of frequency response functions, and calculates the stiffness matrix and reductions in explicit form. A simple helicopter rotor blade was numerically demonstrated for the verification of the proposed method.

A cracked beam is analyzed for the natural frequencies and mode shapes by Zheng and Kessissoglou [72] using finite element method. The study results are compared with the analytical results obtained from local additional flexibility matrix.

Sekhar and Prabhu [73] studied the transient vibration of a cracked rotor which is passing through the critical speed. The study confirmed that the model can be analyzed for the further results like, time histories with harmonics, and frequency spectrum.

On the remark of "The determination of the compliance coefficients at the crack section of a uniform beam with circular cross-section", Abraham et al. [74] studied analytically the double integrals which are commonly encountered when the crack depth exceeds beyond the radius of the cracked section.

Analysis of a rotating cracked shaft to identify the crack depth and crack location with the application of a new method was carried by Gounaris and Papadopoulos [75]. A rotating Timoshenko beam is modelled as a shaft with the gyroscopic effects and axial vibration. The method is used by the authors to find the axial vibration response.

A dynamic study of multi-beams with a transverse crack was carried by Saavedra and Cuitiño [76]. Based on the LFM theory, the additional flexibility of the crack was evaluated by using strain energy density function. The dynamic response of a cracked free-free beam and a U-frame was studied with a harmonic force.

Nayfeh and Mook [77] emphasized the physical aspects of non-linear systems in detail.

2.3. Summary

With the help of web-based tool, research articles related to dynamics of rotor-bearing systems are studied and found that most of them are focused on the rotation of shaft of uniform cross-section with and without crack. The area involving rotations of shaft with variable cross section are less explored. There is a wide scope of research in the area of dynamics of rotor-bearing system with variable cross section with and without crack. The study of the proposed system is carried with mathematical model to understand the system behaviour. Convergence study is done to ensure the system natural whirl frequencies. Besides, Houbolt's implicit time integration scheme is used to study the effect of spin speed with disk eccentricity. The objective of the present work is to obtain the critical speed, unbalance response, natural whirls and stability thresholds for the multi disk, variable cross section rotor-bearing system with transverse crack.

Chapter-3

Theoretical analysis

The dynamic analysis of rotating machineries is generally carried out with the help of vibration measurements and through continuous monitoring of the system. However, some issues are difficult to identify and evaluate purely through measurement based analysis. There are several mathematical methods available to analyse the dynamic behaviour of the rotor bearing system. Out of these methods finite element method plays an important role for the rotating system analysis. The current chapter incorporates the modelling of a rotor-bearing system with Finite Element Method.

Rotor system configuration and interrelate segments

By using Lagrangian formula the finite equation of motion of the rotor shaft element, bearings and rigid disks are developed. Shape functions are derived by using Euler-Bernoulli beam theory. The mathematical expressions for the system with damping and transverse crack are also presented in the following topics.

3.1 System Equation of Motion without crack

The flexible rotor-bearing system is analyzed by finite element method for a typical configuration. The system consists of rotor and collection of discrete disks. Rotor sections are represented with distributed mass and elasticity with discrete bearings. Fig. 3.1 shows the system along with two reference frames (fixed and rotating) that are utilized to describe the systems equation of motion.

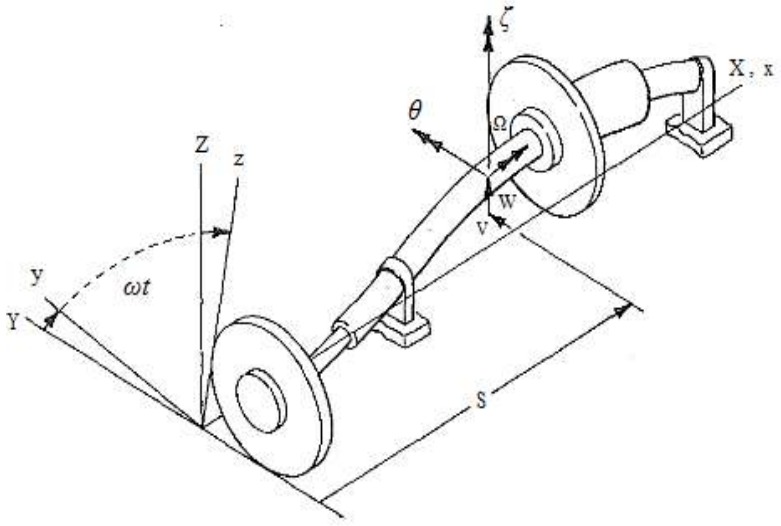

Figure 3.1 Typical Rotor-bearing-disk system configurations.

The rotating frame of reference and fixed frame of references are represented by xyz and XYZ triad respectively. The undeformed rotor, which is represented by X and x axes are collinear and coincident. The rotating frame of reference is defined to fixed frame of reference by a single rotation 'ωt' about X with ω denoting the whirl speed.

A typical cross section of the rotor in a deformed state is defined relative to fixed frame (XYZ) by the translations $V(s, t)$ and $W(s, t)$ in the Y and Z directions respectively to locate the elastic centreline. The small angle rotation $\theta(s, t)$ and $\zeta(s, t)$ about Y and Z axis represents the position of plane of the cross-section respectively. The triad *abc* is attached with the axis '*a*' normal to the plane cross-section represented in Fig. 3.2.

The angular velocities related to the fixed reference frame XYZ can be given as

$$\begin{Bmatrix} \omega_a \\ \omega_b \\ \omega_c \end{Bmatrix} = \begin{bmatrix} -\sin\theta & 1 & 0 \\ \cos\theta \sin\varepsilon & 0 & \cos\varepsilon \\ \cos\theta \cos\varepsilon & 0 & -\sin\varepsilon \end{bmatrix} \begin{Bmatrix} \dot{\zeta} \\ \dot{\varepsilon} \\ \dot{\theta} \end{Bmatrix} \tag{3.1}$$

- ζ about Z defines $a'' b'' c''$
- θ about b'' defines $a' b' c'$
- ε about a' defines $a\ b\ c$

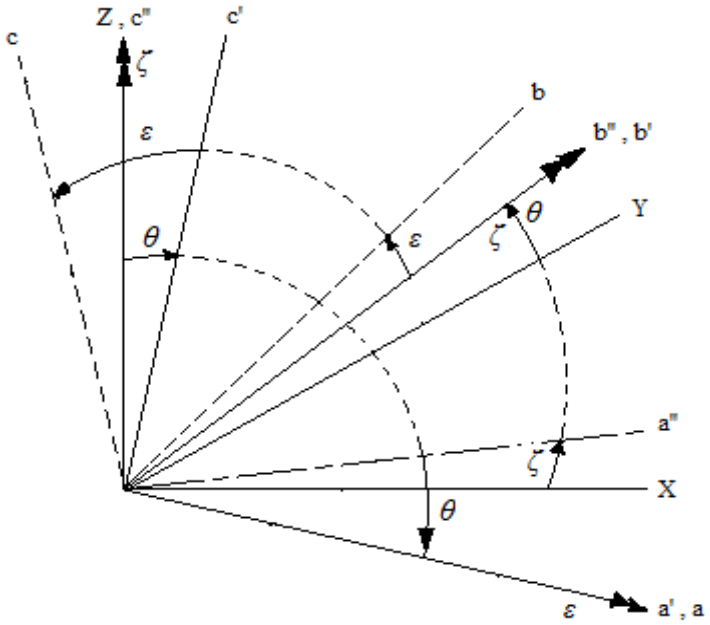

Figure 3.2 Cross section rotation angles

For small deformations, the rotations θ, ζ are approximately collinear with the Y, Z axes respectively. The spin angle ε is constant for a spin speed system with negligible torsional deformation Ωt, where, Ω denotes rotor spin speed. The displacements (V, W, θ, ζ) of a typical cross section related to fixed reference frame are transformed to corresponding displacements (v, w, β, γ) related to rotating reference frame by the orthogonal transformation

$$\{q\} = [R]\{p\} \tag{3.2}$$

With

$$\{q\} = \begin{Bmatrix} V \\ W \\ \theta \\ \zeta \end{Bmatrix}, \{p\} = \begin{Bmatrix} v \\ w \\ \beta \\ \gamma \end{Bmatrix}, [R] = \begin{bmatrix} \cos\omega t & -\sin\omega t & 0 & 0 \\ \sin\omega t & \cos\omega t & 0 & 0 \\ 0 & 0 & \cos\omega t & -\sin\omega t \\ 0 & 0 & \sin\omega t & \cos\omega t \end{bmatrix}. \tag{3.3}$$

After the first and the second derivatives of the equation (3.3) with respect to time can be obtained as,

$$\{\dot{q}\} = \omega[S]\{p\} + [R]\{\dot{p}\} \tag{a}$$

$$\{\ddot{q}\} = [R]\{\{\ddot{p}\} - \omega^2\{p\}\} + 2\omega[S]\{\dot{p}\} \tag{b}$$

With (3.4)

$$[S] = \frac{1}{\omega}[\dot{R}] = \begin{bmatrix} -\sin\omega t & -\cos\omega t & 0 & 0 \\ \cos\omega t & -\sin\omega t & 0 & 0 \\ 0 & 0 & -\sin\omega t & -\cos\omega t \\ 0 & 0 & \cos\omega t & -\sin\omega t \end{bmatrix} \tag{c}$$

The shaft is considered as an Euler-Bernoulli type of beam. Any transverse plane of the beam before bending is assumed to remain plane after bending and remain normal to elastic axis. Therefore, the beam cross section has not only translation but also rotation. The shaft is assumed to have uniformly distributed mass and elasticity. The nodal displacements are the function of time q(t). Four boundary conditions are needed to obtain the shape functions.

$V(0,t) = q_1(t)$ $\quad\quad$ $\zeta(0,t) = q_4(t)$

$V(l,t) = q_5(t)$ $\quad\quad$ $\zeta(l,t) = q_8(t)$

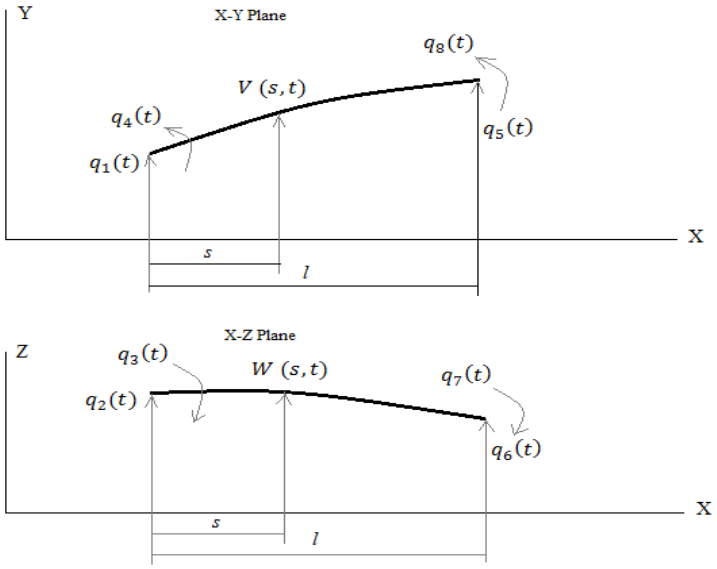

Figure 3.2.1. Relationship between slope and displacements

3.1.1 Undamped flexible finite rotor shaft element

A typical finite rotor element is shown in Fig. 3.3. Here it is assumed that the nodal cross sectional displacements (*V, W*, *θ, ζ*) are assumed to be time dependent and also the function of position (*s*) throughout the element axis. The rotations (*θ, ζ*) are related with translations (*V, W*).

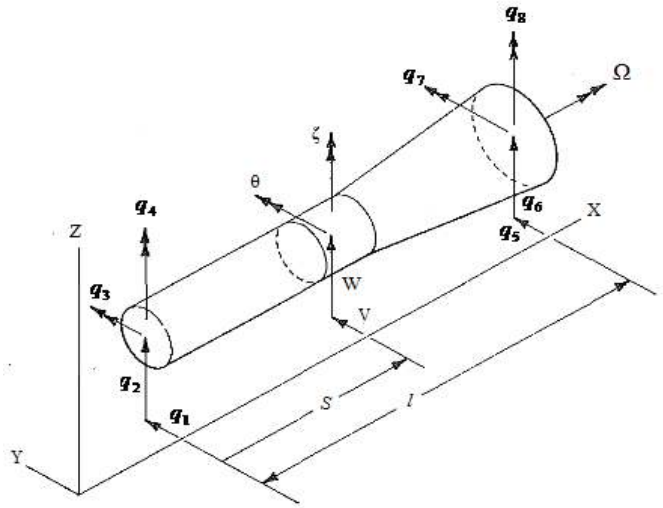

Figure 3.3 Finite rotor element and coordinates

The relation between these two can be expressed by the equation as

$$\theta = -\frac{\partial W}{\partial s} \qquad (3.5)$$
$$\zeta = \frac{\partial V}{\partial s} \quad .$$

The coordinates ($q_1^e, q_2^e \ldots\ldots q_8^e$) are time dependent end point displacements (translations and rotations) which are shown in Fig. 3.3. A spatial shape function is used to express the displacement of each node by using Euler-Bernoulli beam theory. The nodal displacement is a function of time, *q(t)*. The translation of a typical point internal to the element is chosen to obey the relation

$$\begin{Bmatrix} V(s,t) \\ W(s,t) \end{Bmatrix} = [\Psi(s)]\{q^e(t)\} \qquad (3.6)$$

Figure 3.4 illustrates the shaft cross section at displaced position. An infinitesimal area of radial thickness '*dr*' at a distance *r* ($0 \le r \le r_0$) is considered which is subtending an angle *d(Ωt)*. Ω is the rotational speed of the system in rad/sec and '*Ωt*' is the subtended angle varies from 0 to 2π.

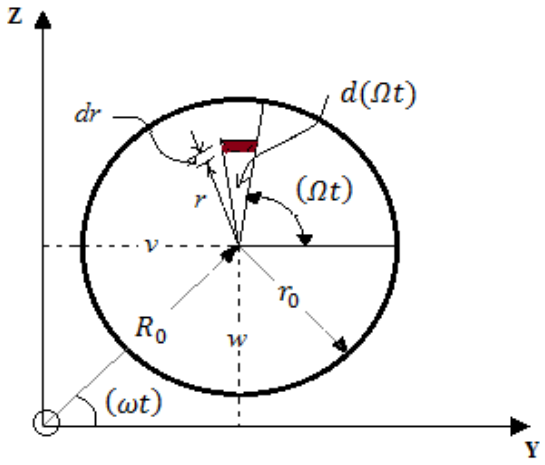

Figure 3.4 Displaced position of the shaft cross-section

The spatial constraint matrix for translation can be written as [11]

$$[\Psi] = \begin{bmatrix} N_1 & 0 & 0 & N_2 & N_3 & 0 & 0 & N_4 \\ 0 & N_1 & -N_2 & 0 & 0 & N_3 & -N_4 & 0 \end{bmatrix} \tag{3.7}$$

Where

$$N_1 = 1 - 3\beta^2 + 2\beta^3; N_2 = L(\beta - 2\beta^2 + \beta^3)$$
$$N_3 = 3\beta^2 - 2\beta^3; N_4 = L(-\beta^2 + \beta^3) \text{ and } \beta = \frac{s}{l}.$$

By using equations (3.5) & (3.6) the rotations for the system can be expressed as,

$$\begin{Bmatrix} \theta \\ \zeta \end{Bmatrix} = [\Phi]\{q^e\} \tag{3.8}$$

With

$$[\Phi] = \begin{bmatrix} [\Phi_\theta] \\ [\Phi_\zeta] \end{bmatrix} = \begin{bmatrix} 0 & -N_1' & N_2' & 0 & 0 & -N_3' & N_4' & 0 \\ N_1' & 0 & 0 & N_2' & N_3' & 0 & 0 & N_4' \end{bmatrix} \tag{3.9}$$

Where, $N_1' = \frac{1}{l}(-6\beta + 6\beta^2); N_2' = 1 - 4\beta + 3\beta^2;$

$$N_3' = \frac{1}{l}(6\beta - 6\beta^2); N_4' = -2\beta + 3\beta^2;$$

3.1.2 Energy equations

Lagrange's equation provides a general formulation for the equation of motion of a dynamical system. The Hamilton's principle can be used to derive the Lagrange's equation in a set of generalized coordinates $'q_i'$. The coordinates are selected as the variables that determine the position of the system. The Lagrange equation for a system can be expressed with kinetic and potential energies as

$$\frac{d}{dt}\left(\frac{\partial T_S}{\partial \dot{q}_i}\right) - \left(\frac{\partial T_S}{\partial q_i}\right) + \left(\frac{\partial U_S}{\partial q_i}\right) + \left(\frac{\partial D}{\partial \dot{q}_i}\right) = Q_i \tag{3.10}$$

Where *i=1, 2...n., 'T_S'* is the total kinetic energy, 'U_S' is the total potential energy, *D'* is the Rayleigh's dissipation function and $'Q_i'$ is the virtual work done on the system.

$$\delta W = \sum_{i=1}^{n} Q_i \delta q_i \tag{3.11}$$

The Lagrangian equation gives a group of second order ordinary differential equations. These equations are non-linear and non-homogeneous. For the differential disk which is located at the position (*s*) along the axial direction, the elastic bending and kinetic energy is expressed as

$$\begin{aligned} &P.E:\ d\mathcal{P}_B^e = \tfrac{1}{2}\begin{Bmatrix} v'' \\ w'' \end{Bmatrix}^T \begin{bmatrix} EI & 0 \\ 0 & EI \end{bmatrix} \begin{Bmatrix} v'' \\ w'' \end{Bmatrix} ds \quad and \\ &K.E:\ d\mathcal{J}^e = \tfrac{1}{2}\begin{Bmatrix} \dot{v} \\ \dot{w} \end{Bmatrix}^T \begin{bmatrix} \mu & 0 \\ 0 & \mu \end{bmatrix} \begin{Bmatrix} \dot{v} \\ \dot{w} \end{Bmatrix} ds + \tfrac{1}{2}\dot{\varepsilon}^2 \mathcal{I}_P\, ds + \tfrac{1}{2}\begin{Bmatrix} \dot{\theta} \\ \dot{\zeta} \end{Bmatrix}^T \begin{bmatrix} I_D & 0 \\ 0 & I_D \end{bmatrix} \begin{Bmatrix} \dot{\theta} \\ \dot{\zeta} \end{Bmatrix} ds - \dot{\varepsilon}\dot{\zeta}\theta \mathcal{I}_P\, ds\ . \end{aligned} \tag{3.12}$$

Using equations (3.6), (3.8) & (3.12) the potential and kinetic energies of the shaft elements can be written as,

$$\begin{aligned} &P.E:\ d\mathcal{P}_B^e = \tfrac{1}{2} EI\, \{q^e\}^T [\Psi'']^T [\Psi''] \{q^e\}\, ds \qquad and \\ &K.E:\ d\mathcal{J}^e = \tfrac{1}{2}\mu \{\dot{q}^e\}^T [\Psi]^T [\Psi] \{\dot{q}^e\} ds + \tfrac{1}{2}\dot{\phi}^2 \mathcal{I}_P\, ds + \tfrac{1}{2}\, \mathcal{I}_D \{\dot{q}^e\} [\Phi]^T [\Phi] \{\dot{q}^e\}\, ds \\ &\qquad\qquad - \dot{\phi}\mathcal{I}_P \{\dot{q}^e\}^T \left[\Phi_\zeta\right]^T [\Phi_\theta] \{q^e\}\, ds\ . \end{aligned} \tag{3.13}$$

The total potential and kinetic energies of the complete element is obtained by integrating the equations (3.13) over the length of the shaft element which is obtained as,

$$\mathcal{P}_B^e + \mathcal{J}^e = \frac{1}{2}\{q^e\}^T[K_B^e]\{q^e\} + \frac{1}{2}\{\dot{q}^e\}^T([M_T^e]+[M_R^e])\{\dot{q}^e\} + \frac{1}{2}I_P^e\dot{\varepsilon}^2 + \{\dot{q}^e\}^T[N^e]\{\dot{q}^e\} \quad (3.14)$$

Where

$$[M_T^e] = \int_0^l \mu[\Psi]^T[\Psi]\,ds \quad (a)$$

$$[M_R^e] = \int_0^l \mathcal{I}_D[\Phi]^T[\Phi]\,ds \quad (b)$$

$$[N^e] = \int_0^l \mathcal{I}_P\left[\Phi_\zeta\right]^T[\Phi_\theta]\,ds \quad (c)\ (3.15)$$

$$[K_B^e] = \int_0^l EI\,[\Psi'']^T[\Psi'']\,ds \quad (d)$$

$$[G^e] = ([N^e] - [N^e]^T) \quad (e)$$

The Lagrangian equation of motion for the finite rotor shaft element using the equation (3.14) and the constant rotational speed restriction, $\dot{\varepsilon} = \Omega$ can be written as

$$([M_T^e] + [M_R^e])\{\ddot{q}^e\} - \Omega[G^e]\{\dot{q}^e\} + ([K_B^e])\{q^e\} = \{Q^e\} \quad (3.16)$$

The force vector $\{Q^e\}$ includes the unbalance mass, interconnection forces, and other element external effects. For the shaft element with distributed mass center eccentricity $(\eta(s), \zeta(s))$, the equivalent unbalance force using the consistent matrix approach can be expressed as [11]

$$\{Q^e\}_{8x1} = \{Q_c^e\}\cos(\Omega t) + \{Q_s^e\}\sin(\Omega t) \quad (3.17)$$

3.1.2.1 Rigid Disk

The disk for the analysis is assumed to be axisymmetric and rigid with rotational and translational motion. The total kinetic energy of the system is represented by the sum of the rotational and translational kinetic energies. Using the Lagrange method the kinetic energy is given by the following expression,

$$T_d = \frac{1}{2}\begin{Bmatrix}\dot{V}\\ \dot{W}\end{Bmatrix}^T\begin{bmatrix}m_d & 0\\ 0 & m_d\end{bmatrix}\begin{Bmatrix}\dot{V}\\ \dot{W}\end{Bmatrix}+\frac{1}{2}\begin{Bmatrix}\omega_a\\ \omega_b\\ \omega_c\end{Bmatrix}^T\begin{bmatrix}I_D & 0 & 0\\ 0 & I_D & 0\\ 0 & 0 & I_D\end{bmatrix}\begin{Bmatrix}\omega_a\\ \omega_b\\ \omega_c\end{Bmatrix} \tag{3.18}$$

By using equation (3.1), equation (3.18) becomes,

$$T_d = \frac{1}{2}\begin{Bmatrix}\dot{V}\\ \dot{W}\end{Bmatrix}\begin{bmatrix}m_d & 0\\ 0 & m_d\end{bmatrix}\begin{Bmatrix}\dot{V}\\ \dot{W}\end{Bmatrix}+\frac{1}{2}\begin{Bmatrix}\dot{\theta}\\ \dot{\zeta}\end{Bmatrix}^T\begin{bmatrix}I_D & 0\\ 0 & I_D\end{bmatrix}\begin{Bmatrix}\dot{\theta}\\ \dot{\zeta}\end{Bmatrix}-\dot{\varepsilon}\dot{\zeta}\theta I_p \tag{3.19}$$

$$\frac{d}{dt}\left(\frac{\partial T}{\partial \dot{q}}\right)-\left(\frac{\partial T}{\partial q}\right)=[M^d]\{\ddot{q}\}-\Omega\,[G^d]\{\dot{q}\} \tag{3.20}$$

The Lagrangian equation of motion of the rigid disk for the constant spin speed restriction ($\dot{\varepsilon}=\Omega$) equation (3.20) will become

$$([M_T^d]+[M_R^d])\{\ddot{q}^d\}-\Omega[G^d]\{\dot{q}^d\}=\{Q^d\} \tag{3.21}$$

The equation (3.21) is the equation of motion of the rigid disk referred to the fixed frame of reference with the forcing term including mass unbalance, interconnection forces, and other external effects on the disk. By using the equations (3.2-3.4) and pre-multiplying by $[R]^T$, equation (3.21) is transformed to the form of,

$$([M_T^d]+[M_R^d])\{\ddot{p}^d\}+\omega(2([\hat{M}_T^d]+[\hat{M}_R^d])-\lambda[G^d])\{\dot{p}^d\}-\omega^2(([M_T^d]+[M_R^d])+\lambda[\hat{G}^d])\{p^d\}=\{P^d\} \tag{3.22}$$

For the case of thin disc $(I_P=2I_D)$ equation (3.22) become,

$$([M_T^d]+[M_R^d])\{\ddot{p}^d\}+\omega(2[\hat{M}_T^d]+(1-\lambda)[G^d])\{\dot{p}^d\}-\omega^2([M_T^d]+(1-2\lambda)[M_R^d])\{p^d\}=\{P^d\} \tag{3.23}$$

The equations (3.22) and (323) are the equation of motion of a rigid disc referred to rotating frame with whirl ratio $\lambda=\Omega/\omega$.

3.1.2.2 Bearings

The virtual work of the forces acting on the shaft can be written as,

$$\delta W = -k_{VV}^{b} V\delta V - k_{VW}^{b} W\delta V - k_{WW}^{b} W\delta W - k_{WV}^{b} V\delta W - c_{VV}^{b}\dot{V}\delta V - c_{VW}^{b}\dot{W}\delta V - c_{WW}^{b}\dot{W}\delta W - c_{WV}^{b}\dot{V}\delta W \quad (3.24)$$

The equation (3.24) can be expressed by the following relation,

$$\delta W = F_V \delta_V + F_W \delta_W \quad (3.25)$$

By neglecting the influence of slopes and bending moments the main characteristic link forces will become

$$F_V = -k_{VV}^{b} V - k_{VW}^{b} W - c_{VV}^{b}\dot{V} - c_{VW}^{b}\dot{W} \quad (3.26)$$

$$F_W = -k_{WW}^{b} W - k_{WV}^{b} V - c_{WW}^{b}\dot{W} - c_{WV}^{b}\dot{V} \quad (3.27)$$

Representing in matrix form, the equation (3.26) and (3.27) can be expressed as

$$\begin{bmatrix} F_V \\ F_\theta \\ F_W \\ F_\zeta \end{bmatrix} = -\begin{bmatrix} k_{VV}^{b} & 0 & k_{VW}^{b} & 0 \\ 0 & 0 & 0 & 0 \\ k_{WV}^{b} & 0 & k_{WW}^{b} & 0 \\ 0 & 0 & 0 & 0 \end{bmatrix}\begin{bmatrix} V \\ \theta \\ W \\ \zeta \end{bmatrix} - \begin{bmatrix} c_{VV}^{b} & 0 & c_{VW}^{b} & 0 \\ 0 & 0 & 0 & 0 \\ c_{WV}^{b} & 0 & c_{WW}^{b} & 0 \\ 0 & 0 & 0 & 0 \end{bmatrix}\begin{bmatrix} \dot{V} \\ \ddot{\theta} \\ \dot{W} \\ \dot{\zeta} \end{bmatrix} \quad (3.28)$$

The system is subjected to only one type of interconnecting component which is the bearings. These bearings are linearized and the stiffness only considered in the analysis. The equation of motion of the bearings as follows,

$$\left(\frac{\partial D}{\partial \dot{q}}\right) + \frac{\partial U}{\partial q} = [C^b]\{\dot{q}^b\} + [K^b]\{q^b\} \quad (3.29)$$

$$[C^b]\{\dot{q}^b\} + [K^b]\{q^b\} = \{Q^b\} \quad (3.30)$$

Where,

$$[K^b] = \begin{bmatrix} k_{VV}^{b} & k_{VW}^{b} \\ k_{WV}^{b} & k_{WW}^{b} \end{bmatrix} \text{ and } [C^b] = \begin{bmatrix} c_{VV}^{b} & c_{VW}^{b} \\ c_{WV}^{b} & c_{WW}^{b} \end{bmatrix}.$$

3.1.3 Rotor element with variable cross section

Figure 3.5 shows the variable cross sectional properties of a typical rotor shaft element. For these elements the equation of motion can be obtained by either evaluating the integrals of the equations (3.15) and (3.17) by using the variable properties of the system.

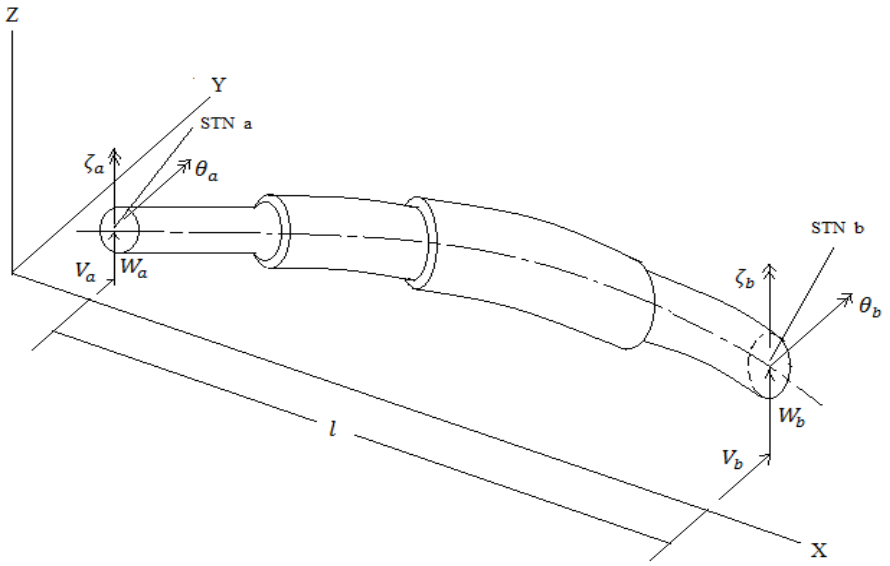

Figure 3.5 Sub-elements assemblage

Then the set of assembled sub elements possesses [4 x (total number of sub element stations)] coordinates which can be reduced by following procedure.

The sub element equations in the assembled form, in fixed frame coordinate can be represented as

$$\left(\left[M_T^e\right]+\left[M_R^e\right]\right)\begin{Bmatrix}\{\ddot{q}^e\}_a\\ \{\ddot{q}^e\}_b\\ \{\ddot{q}^e\}_c\end{Bmatrix}-\Omega\left[G^e\right]\begin{Bmatrix}\{q^e\}_a\\ \{q^e\}_b\\ \{q^e\}_c\end{Bmatrix}+\left[K_B^e\right]=\{Q^e\} \tag{3.31}$$

The internal displacements $\{q^e\}_b$ and the end point displacements of the element $\{q^e\}_a$ and $\{q^e\}_c$ are having the displacement dependency between them. Thus, this can be adopted by considering the static, homogeneous case of the previous equation (3.31).

$$\begin{bmatrix} [K^e]_{aa} & [K^e]_{ab} & [K^e]_{ac} \\ [K^e]_{ba} & [K^e]_{bb} & [K^e]_{bc} \\ [K^e]_{ca} & [K^e]_{cb} & [K^e]_{cc} \end{bmatrix} \begin{Bmatrix} \{q^e\}_a \\ \{q^e\}_b \\ \{q^e\}_c \end{Bmatrix} = \{0\} \tag{3.32}$$

From the second row of equation (3.32), the internal displacement vector $\{q^e\}_b$ can be written as

$$\{q^e\}_b = -[K^e]_{bb}^{-1}[K^e]_{ba}\{q^e\}_a - [K^e]_{bb}^{-1}[K^e]_{bc}\{q^e\}_c \tag{3.33}$$

The following constraint of equation can be written by using the equation (3.33)

$$\begin{Bmatrix} \{q^e\}_a \\ \{q^e\}_b \\ \{q^e\}_c \end{Bmatrix} = \begin{bmatrix} [I] & [0] \\ -[K^e]_{bb}^{-1}[K^e]_{ba} & -[K^e]_{bb}^{-1}[K^e]_{bc} \\ [0] & [I] \end{bmatrix} \begin{Bmatrix} \{q^e\}_a \\ \{q^e\}_c \end{Bmatrix} \tag{3.34}$$

From the equation (3.34), the elements in the columns of the constraint matrix represents the static mode shapes. By applying the equation (3.34) to the equation (3.31) it reduces the number of coordinates and associated components of force to eight, and this provides the same element equation form as the equation (3.16). In this research work, reduction of co-ordinates technique [11] is used to model the rotor elements having variable cross section.

3.1.4 Undamped system equation of motion

The undamped system equation of motion in the assembled form which consisting of the component equations form the equation (3.16), (3.21), and (3.30), is of the form,

$$[M^S]\{\ddot{q}^S\} - \Omega[G^S]\{\dot{q}^S\} + [K^S]\{q^S\} = \{Q^S\}_{4n\times 1} \ . \tag{3.35}$$

Where

$[M^S] = [M^e] + [M^d]$; $[G^S] = [G^e] + [G^d]$; $[K^S] = [K_B^e] + [K^b]$; $[M^e] = [M_T^e] + [M_R^e]$ and

$[M^d] = [M_T^d] + [M_R^d]$; $\{q^S\} = \{V_i \ W_i \ \theta_i \ \zeta_i \ V_{i+1} \ W_{i+1} \ \theta_{i+1} \ \zeta_{i+1} \cdots\cdots\cdots N+1\}^T$.

3.1.5 Damped flexible finite rotor shaft element

The previous study is extended to incorporate the internal damping in the finite element formulation. In their finite element formulation Zorzi and Nelson [42] have considered the combined effects of both viscous and hysteretic internal damping of the rotor-bearing system. By using the both η_V and η_H, which denotes the viscous damping coefficient and the hysteretic loss factor of the shaft Material.

The potential energy U^e and kinetic energy T^e of the element, can be given by the nodal displacement vector $\{q^e\}$ as respectively,

$$U^e = \frac{1}{2}\{q_e\}^T [K_B^e]\{q_e\} \tag{3.36}$$

$$T^e = \frac{1}{2}\{\dot{q}_e\}^T ([M_T^e] + [M_R^e])\{\dot{q}_e\} - \Omega\{\dot{q}_e\}^T [N^e]\{q_e\} + \frac{1}{2} I_P l \Omega^2 \tag{3.37}$$

Here, the stress-strain relationship can be expressed as [42],

$$\sigma = E\{\vartheta + \eta_V \dot{\vartheta}\}\vartheta = -r\cos[(\Omega - \omega)t]\frac{\partial^2 R_0(x,t)}{\partial x^2} \quad \text{(a)}$$

(3.38)

$$\dot{\vartheta} = (\Omega - \omega) r \sin[(\Omega - \omega)t]\frac{\partial^2 R_0}{\partial x^2} - r\cos[(\Omega - \omega)t]\frac{\partial}{\partial t}\left(\frac{\partial^2 R_0}{\partial x^2}\right) \quad \text{(b)}$$

It is evident from the equation (3.38, b) that, when the system spin speed and the whirl speed (synchronous state) matches ($\Omega = \omega$), and when the orbit is in circular shape, the term $(\partial/\partial t)(\partial^2 R_0/\partial x^2) = 0,$ besides the component of viscous damping which provides no variation of the axial stress σ of equation (3.38, a). Hence, for the synchronous circular orbits, the component of internal viscous damping can't produce any out of phase loading to reduce the critical speed orbit.

The bending moments at any instant about Y and Z -axes can be expressed as,

$$M_Z = \int_0^{2\pi}\int_0^{r_0} -(V + r\cos(\Omega t))\sigma r dr d(\Omega t) \quad \text{(a)}$$

$$M_Y = \int_0^{2\pi}\int_0^{r_0} (W + r\sin(\Omega t))\sigma r dr d(\Omega t) \quad \text{(b)} \qquad (3.39)$$

The above equations (3.39) for bending moment becomes by substituting the appropriate values and by integrating on the limits,

$$\begin{Bmatrix} M_Z \\ M_Y \end{Bmatrix} = EI\begin{bmatrix} 1 & \eta_V\Omega \\ \eta_V\Omega & -1 \end{bmatrix}\begin{Bmatrix} V'' \\ W'' \end{Bmatrix} + EI\begin{bmatrix} \eta_V & 0 \\ 0 & -\eta_V \end{bmatrix}\begin{Bmatrix} \dot{V}'' \\ \dot{W}'' \end{Bmatrix} \qquad (3.40)$$

It is observed that, the strain energy d P^e and the dissipation function d D^e for an infinitesimal element, by neglecting the shear deformations which can be expressed in the form of

$$dP^e = \frac{1}{2}EI\begin{Bmatrix} \theta' \\ \zeta' \end{Bmatrix}^T [\eta]\begin{Bmatrix} \theta' \\ \zeta' \end{Bmatrix} ds \qquad (3.41)$$

$$dD^e = \frac{1}{2}\eta_V EI\begin{Bmatrix} \dot{\theta}' \\ \dot{\zeta}' \end{Bmatrix}^T \begin{Bmatrix} \dot{\theta}' \\ \dot{\zeta}' \end{Bmatrix} ds \qquad (3.42)$$

$$[\eta] = \begin{bmatrix} \eta_a & \eta_b \\ -\eta_b & \eta_a \end{bmatrix} \quad \text{(a)}$$

$$\eta_a = \frac{1+\eta_H}{\sqrt{1+\eta^2{}_H}} \quad \text{(b)} \qquad (3.43)$$

$$\eta_b = \frac{\eta_H}{\sqrt{1+\eta^2{}_H}} + \Omega\eta_V \quad \text{(c)}$$

By integrating the equations (3.41) and (3.42) over the whole length of the element, the strain energy, 'P^e' and the dissipation function, 'D^e' with internal viscous and hysteretic damping of the shaft element, gives the following set of equations

$$P^e = \frac{1}{2}\eta_a\{q^e\}^T[K_B^e]\{q^e\} + \frac{1}{2}\eta_b\{q^e\}^T[K_D^e]\{q^e\} \qquad (3.44)$$

$$D^e = \frac{1}{2}\eta_V\{\dot{q}^e\}^T[K_B^e]\{\dot{q}^e\} \quad . \qquad (3.45)$$

Where

$$\left[K_D^e\right] = \int_0^l EI[\Psi'']^T[\Psi][\Psi'']ds$$

3.1.6 Damped system equation of motion

Through the use of Hamilton's principle, the Lagrangian equation of motion obtained for the damped finite rotating shaft element in the following matrix form as,

$$\left(\left[M_T^e\right] + \left[M_R^e\right]\right)\left\{\ddot{q}^e\right\} + \left(\eta_V\left[K_B^e\right] - \Omega\left[G^e\right]\right)\left\{\dot{q}^e\right\} + \left(\eta_a\left[K_B^e\right] - \eta_b\left[K_c^e\right]\right)\left\{q^e\right\} = \left\{Q^e\right\} \quad (3.46)$$

From the equation (3.46) all the matrices are symmetric, except the gyroscopic matrix $\left[G^e\right]$ and the circulation matrix $\left[K_c^e\right]$ which are skew symmetric. Here the instabilities resulting from internal dampings are characterized by this circulation matrix $\left[K_c^e\right]$. The material damping which is in the form of viscous, contributes to the circulation effects and also providing a dissipation term $\eta_V\left[K_B^e\right]\left\{\dot{q}^e\right\}$. Due to this nature, it can provide a rotor system in the stable condition, providing that this dissipation term dominates. This form can be achieved, when the rotor system with the undamped isotropic supports and the spin speed is less than the first forward critical speed.

Hence for the damped system equation of motion can be expressed as,

$$\left(\left[M^e\right] + \left[M^d\right]\right)\left\{\ddot{q}^S\right\} + \left(\eta_V\left[K_B^e\right] - \Omega\left(\left[G^e\right] + \left[G^d\right]\right)\right)\left\{\dot{q}^S\right\} + \left(\eta_a\left[K_B^e\right] - \eta_b\left[K_c^e\right]\right)\left\{q^S\right\} = \left\{Q^S\right\} \quad (3.47)$$

3.1.7 System instability regions

Instability regions can be divided into two types: first one is primary instability regions (PIRs) and the second is combination instability regions (CIRs). The starting points of these instability regions for the periodically time-varying system could be expressed in the spinning (rotating speed) axis as [77]

$$\begin{cases} 2\Omega_n^p = \dfrac{2}{n}\omega_i, & n = 1, 2,... \quad \text{for PIRs} \\ 2\Omega_m^p = \dfrac{2}{m}\left(\omega_i + \omega_j\right) & i \neq j,\ m = 1, 2,... \text{ for CIRs} \end{cases}, \tag{3.48}$$

Where ω_i and ω_j are the whirling frequencies of i^{th} and j frequencies of the system. The results from the literatures show that the ω_i and ω_j in the equation (3.48) includes only the forward whirling frequencies. Here $n = 1$ and $m = 1$ has taken for the PIR and CIR respectively. The results for these instability regions are computed for the first and second forward whirling frequencies. The system rotating speed lines are plotted with $\omega_i = \Omega, \omega_i = 2\Omega - \omega_{b1}$ and $\omega_i = 2\Omega - \omega_{f1}$ for the both uncracked and the cracked rotor systems which are presented in the results chapter to figure out the instability regions related to the first two forward natural whirl modes.

3.1.8 Whirl speed analysis

Generally when the rotor shaft is in rotation, the shaft enters into transverse oscillations. The centrifugal force due to the shaft unbalance is responsible for vibration. If the shaft speed matches with the natural frequency of the transverse oscillations, the system vibration behaviour raises and indicates the whirling of the shaft. This shaft whirling will damage the rotating systems. So, it is essential to balance the system very carefully to reduce this effect and to design the system natural frequency for the different spinning speeds. For the computational purpose of the system equation of motion, the eigenvalues can be obtained from the following equation,

$$\begin{bmatrix} [0] & [I] \\ -[K^S]^{-1}[M^S] & \left(\Omega[K^S]^{-1}[G^S]\right) \end{bmatrix} \{h_0\} = \frac{1}{\alpha}\{h_0\} \tag{3.49}$$

The equation (3.49) represents the conjugative pairs of the pure imaginary with the magnitude for the orthotropic bearing which is equal to the system natural whirl speeds.

3.2 Fault modelling in the rotor system

In this research study, two types of faults are considered. First one is unbalance in the rotor rigid disk and the other is transverse crack at the rotor shaft element *j*. The asymmetric angle ϕ, non-dimensional crack depths μ and location of crack are investigated to identify the effects on the instability regions of the system. The modelling of fault is carried as the same way the rotor system was modelled in the previous sessions. This is done by using Lagrangian method.

3.2.1 Linear mass unbalance in rotor

Unbalance in rotor system is unavoidable and it cannot be completely eliminated. It happens when the mass centre of the shaft is misaligned with the rotation centre or bearing centre axis. This makes the rotor to the wobbling motion and major source of vibration. To correct these unbalance, first it is essential to determine the unbalance. The presence of unbalance changes the dynamic behaviour of the rotor system. Linear mass unbalance distribution can be expressed by using the mass center eccentricity.

3.2.1.1 Unbalance Response

When the speed of the rotor bearing system increases, the amplitude is commonly excited by the unbalance forces presents in the system. These vibration amplitudes frequently passes through the maximum speed is called critical speed. When a constant speed is considered the unbalance force for equation (3.39) in the fixed frame coordinates, the equation for the system unbalance force can be given in the relation as [11]

$$\left\{Q^S\right\} = \left\{Q_c^S\right\}\cos(\Omega t) + \left\{Q_s^S\right\}\sin(\Omega t) \tag{3.50}$$

The steady state form of the solution will be,

$$\left\{q^S\right\} = \left\{q_c^S\right\}\cos(\Omega t) + \left\{q_s^S\right\}\sin(\Omega t) \tag{3.51}$$

By substituting the above equations (3.50) and (3.51) in the equation (3.35) yields,

$$\begin{Bmatrix} \{q_c^e\} \\ \{q_s^e\} \end{Bmatrix} = \begin{bmatrix} ([K^S] - \Omega^2[M^S]) & -\Omega^2[G^S] \\ \Omega^2[G^S] & [([K^S] - \Omega^2[M^S])] \end{bmatrix}^{-1} \begin{Bmatrix} \{Q_c^S\} \\ \{Q_s^S\} \end{Bmatrix} \tag{3.52}$$

From the equation (3.52), the solution can be obtained by the back substitution to the equation (3.51), which gives the undamped rotor system unbalance response.

3.2.2 Transverse crack modelling

The present study proposes the vibration analysis of the rotor-bearing system with transverse crack based on the finite element approach. The dynamic behaviour of the rotor-bearing system with periodically time varying stiffness and various crack depths are investigated. The effect of transverse crack on the starting point of instability regions of the rotor-bearing system is also carried out in the analysis. The following section elaborates the finite element equations of motion of the rotor-bearing system with transverse crack.

The transverse crack appears at the shaft element *j* (Fig. 4.10). The relative position of the crack in the circumference is illustrated in the Fig. 3.6.

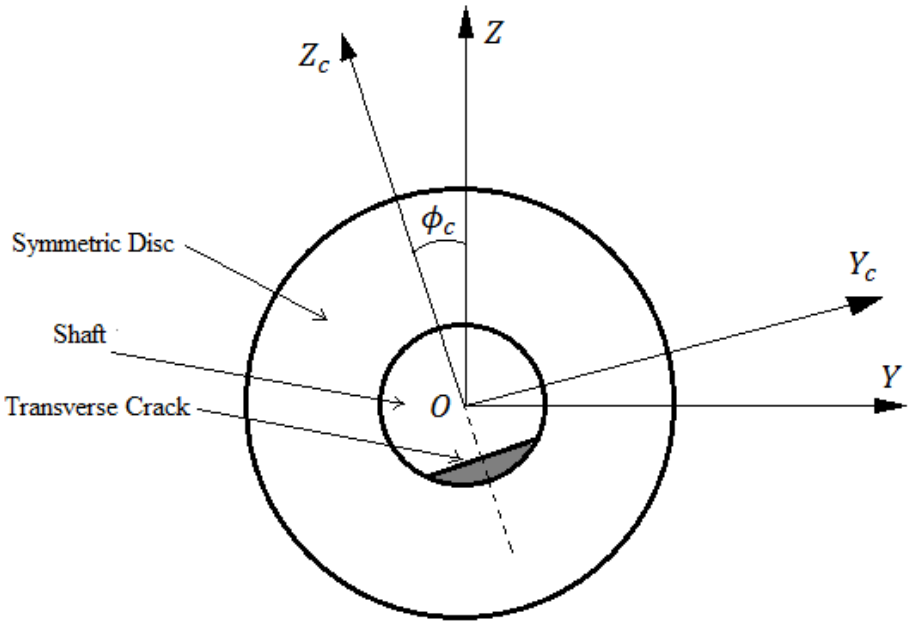

Figure 3.6. Relative positions of the shaft and transverse crack in circumference

The angle between the major axes of the crack and the shaft is shown by ' ϕ_c'. 'ϕ' is called as the asymmetric angle, which is equal to ϕ_c ($\phi_c = \phi$). The asymmetric angle , is an important factor for parametric instability of rotor system. The element matrices for the transverse crack are introduced and derived for the assemblies of the FEM model of the rotor system. In addition to this, a case of transverse crack: an open crack is taken in the derivation. The crack is assumed to be present at an angle of ϕ relative to the fixed negative Z-axis at t = 0, as shown in Figure 3.6. As the shaft starts to rotate the crack angle with respect to the negative Z-axis changes with time to ($\phi + \Omega t$).

3.2.2.1 Transverse crack element modelling

For an open crack case, the stiffness matrix of the cracked element in a generalized form similar to that of the asymmetric rod can be written as [47]

$$\mathbf{k}_{ce}^{j}(t) = \frac{E}{l^3}\begin{bmatrix} 12I_{\bar{Y}}(t) & 0 & 0 & -6lI_{\bar{Y}}(t) & -12I_{\bar{Y}}(t) & 0 & 0 & -6lI_{\bar{Y}}(t) \\ 0 & 12I_{\bar{Z}}(t) & 6lI_{\bar{Z}}(t) & 0 & 0 & -12I_{\bar{Z}}(t) & 6lI_{\bar{Z}}(t) & 0 \\ 0 & 6lI_{\bar{Z}}(t) & 4l^2I_{\bar{Z}}(t) & 0 & 0 & -6lI_{\bar{Z}}(t) & 2l^2I_{\bar{Z}}(t) & 0 \\ -6lI_{\bar{Y}}(t) & 0 & 0 & 4l^2I_{\bar{Y}}(t) & 6lI_{\bar{Y}}(t) & 0 & 0 & 2l^2I_{\bar{Y}}(t) \\ -12I_{\bar{Y}}(t) & 0 & 0 & 6lI_{\bar{Y}}(t) & 12I_{\bar{Y}}(t) & 0 & 0 & 6lI_{\bar{Y}}(t) \\ 0 & -12I_{\bar{Z}}(t) & -6lI_{\bar{Z}}(t) & 0 & 0 & 12I_{\bar{Z}}(t) & -6lI_{\bar{Z}}(t) & 0 \\ 0 & 6lI_{\bar{Z}}(t) & 2l^2I_{\bar{Z}}(t) & 0 & 0 & -6lI_{\bar{Z}}(t) & 4l^2I_{\bar{Z}}(t) & 0 \\ -6lI_{\bar{Y}}(t) & 0 & 0 & 2l^2I_{\bar{Y}}(t) & 6lI_{\bar{Y}}(t) & 0 & 0 & 4l^2I_{\bar{Y}}(t) \end{bmatrix} \quad (3.53)$$

From equation (3.53), l represents the element length, E is the elastic modulus. The expressions for the time-varying quantities $I_{\bar{Y}}(t)$ and $I_{\bar{Z}}(t)$ are given in the following consequent sections.

3.2.2.2 Open crack

The factors $I_{\bar{Y}}(t)$ and $I_{\bar{Z}}(t)$ are put to the time-varying quantities of the open crack. The expressions for the time-varying quantities $I_{\bar{Y}}(t)$ and $I_{\bar{Z}}(t)$ are considered as [47],

$$I_{\bar{Y}}(t) = I_1 + I_2 \cos(2(\Omega t + \varphi)) \quad \text{(a)}$$

$$I_{\bar{Z}}(t) = I_1 - I_2 \cos(2(\Omega t + \varphi)) \ . \quad \text{(b)} \qquad (3.54)$$

Where $I_1 = \frac{1}{2}\ (I_Y + I_Z - A_1 e^2)$ and $I_2 = \frac{1}{2}\ (I_Y - I_Z - A_1 e^2)$. These variables are constant quantities throughout the time of the shaft rotation. By considering the profile of the cracked element cross-section, the following quantities can be obtained by deploying the non-dimensional crack depth ($\mu = h/R$), and the shaft radius (R) as,

$$I_Y = \frac{\pi R^4}{8} + \frac{R^4}{4}\left((1-\mu)\left(2\mu^2 - 4\mu + 1\right)\gamma + \sin^{-1}(1-\mu)\right) \qquad (3.55)$$

$$I_Z = \frac{\pi R^4}{4} - \frac{R^4}{12}\left((1-\mu)\left(2\mu^2 - 4\mu - 3\right)\gamma + 3\sin^{-1}(\gamma)\right) \qquad (3.56)$$

$$A_1 = R^2\left(\pi - \cos^{-1}(1-\mu) + (1-\mu)\gamma\right) \qquad (3.57)$$

$$e = \frac{2R^3}{3A_1}\gamma^3 \qquad (3.58)$$

Where $\gamma = \sqrt{\mu(2-\mu)}$. Hence the finite element stiffness matrix for the j^{th} element with open crack can be given as,

$$\mathbf{k}_{oc}^{j}(t) = \mathbf{k}_{o1}^{j} + \mathbf{k}_{o2}^{j} \cos(2(\Omega t + \phi)) \qquad (3.59)$$

The equation (3.59) represents the time-periodic stiffness matrix with frequency of 2Ω.

3.2.2.3 Equation of motion of the system with transverse open crack

The global equation of motion for the rotor-bearing system with the transverse open crack can be written in fixed frame coordinates by neglecting the unbalance force as

$$[M^S]\{\ddot{q}^S(t)\} - \Omega[G^S]\{\dot{q}^S(t)\} + ([K^S] + [\tilde{K}(t)])\{q^S(t)\} = 0 \qquad (3.60)$$

Where, $[M^S]$ = global mass matrix

$[G^S]$ = global gyroscopic matrix

$[K^S]$ = global stiffness matrix of the un-cracked rotor-bearing system equal to $\mathbf{k}_{o1}^{j}$

$$\left[\widetilde{K}(t)\right] = \left[\widetilde{K}_o\right]\cos 2(\Omega t + \phi)$$

$\left[\widetilde{K}_o\right]$ = global stiffness matrix of the cracked element, equal to $\mathbf{k}_{o2}^{j}$.

$\left\{q^S(t)\right\} = \left\{q_1^e \ldots\ldots\ldots q_i^e, \ldots\ldots\ldots q_{N+1}^e\right\}^T$ is the global displacement vector.

The matrices $\left[M^S\right]$, $\left[G^S\right]$, $\left[K^S\right]$ and $\left[\widetilde{K}(t)\right]$ are having the dimensions of 4(N+1) x 4(N+1). The equation of motion of the system is a second order differential equation with frequency of 2Ω for the open crack. This system is periodically time-varying.

3.3.3 Lateral displacement responses of bearing using ANSYS

The variable cross-section rotor-bearing system is modelled with axisymmetric elements (SOLID273) to determine the bearing response. These elements possess the variable cross sections of rotor sections with impulse excitations along the X-axis at a node situated in the left overhung part of the rotor. Translational and rotational DOFs about the axis of rotation at the bearing locations are constrained. Fixed support conditions are applied to the nodes of the bearing elements. The rotor-bearing system of axisymmetric elements is given in Figure 3.7 which is developed in ANSYS-*v*13. The analysis was carried out using the commercial ANSYS software package. The axisymmetric rotor was modelled as a configuration of eight master plane nodes. Two undamped linear bearings were located at nodes nine and fifteen respectively as shown in Figure 4.1.1 (c). Modal analysis is performed on rotor bearing system with multiple load steps to determine the natural frequencies and mode shapes.

SOLID273 is used to model axisymmetric solid structures. The element has quadratic displacement behaviour on the master plane and is well suited to modelling irregular meshes on the master plane. The plane on which quadrilaterals or triangles are

defined is called the master plane. It is defined by eight nodes on the master plane, and nodes created automatically in the circumferential direction based on the eight master plane nodes. The element has plasticity, hyper elasticity, stress stiffening, large deflection, and large strain capabilities. The proposed system under considered for analysis is overhung.

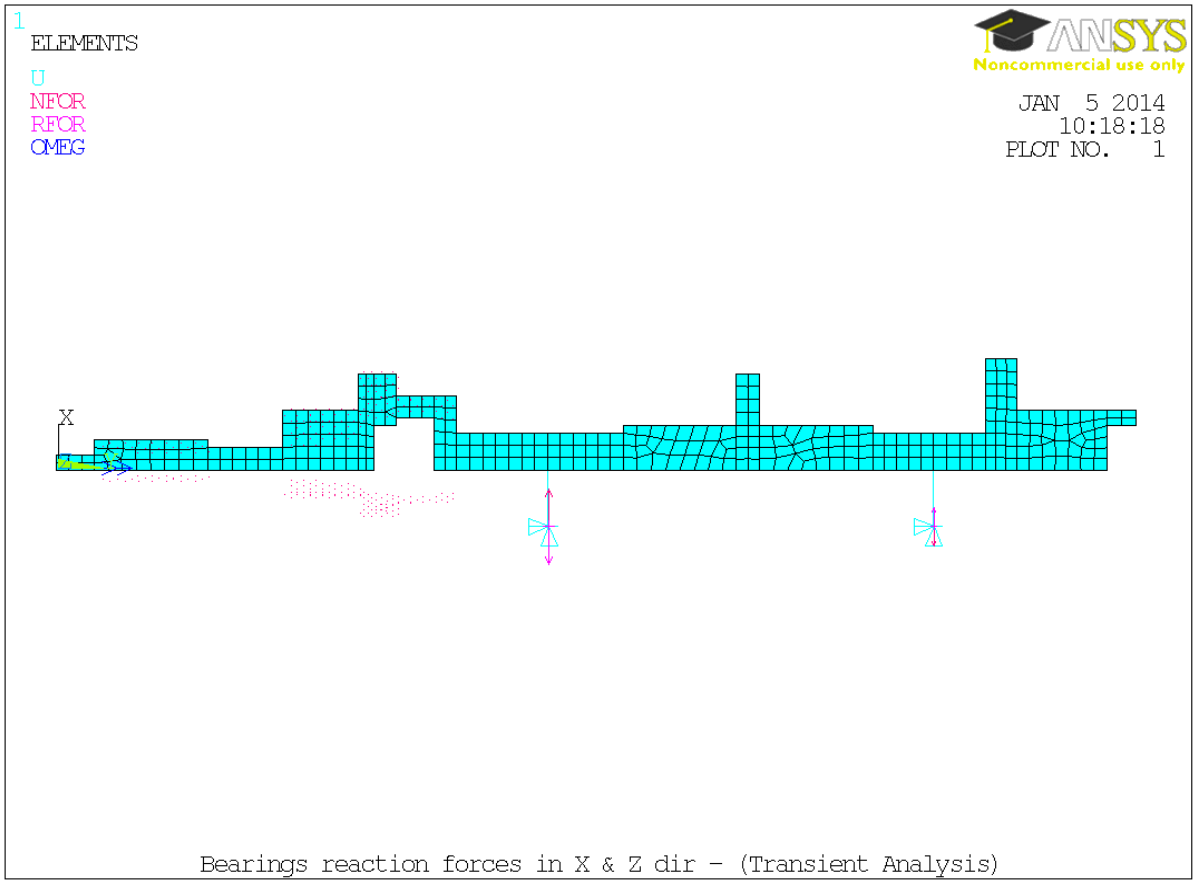

Figure 3.7 Rotor-bearing system with SOLID273 axisymmetric elements

Chapter-4

Numerical Analysis and Discussions

For numerical analysis a rotor bearing system is considered which is represented in Fig. 4.1. The system has variable cross sections along longitudinal direction and is modelled as seven stations which have eighteen sub elements. The rotating shaft is supported by two linear identical bearings which are located at stations four and six respectively. Two disks are placed at stations three and five for analysis.

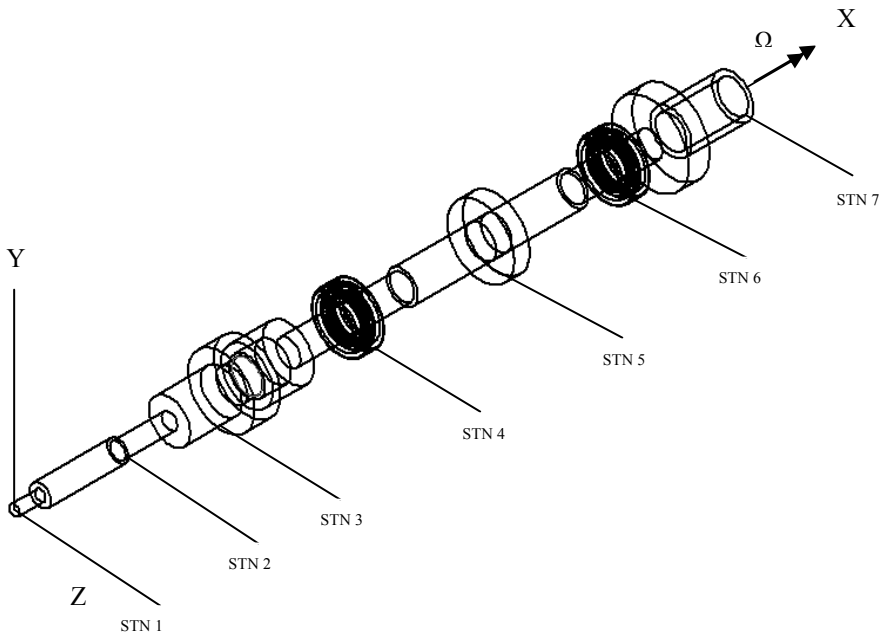

Figure 4.1 Rotor elements with variable cross section

The natural whirl frequencies, mode shapes, unbalance response, critical speeds, natural whirl speeds and frequency responses with phase-plane diagrams of the system are analysed by using finite element method. The effects of hysteresis damping and viscous damping on the above parameters are also discussed. The design variables for the various

cross sections of rotor elements are listed in Table. 4.1. The total length of the typical rotor bearing system is taken as 353 mm. The relative positions of disk-1 and disk-2 are 0.28 and 0.66 respectively from the left end of the system.

Table 4.1 Rotor element configuration data

Station No.	Node No.	Axial Dist (cm)	Inner Dia. (cm)	Outer Dia. (cm)
1	1	0.00		0.51
	2	1.27		1.02
2	3	5.08		0.76
	4	7.62		2.03
3	5	8.89		2.03
	6	10.16		3.30
	7	10.67	1.52	3.30
	8	11.43	1.78	2.54
	9	12.70		2.54
	10	13.46		1.27
4	11	16.51		1.27
	12	19.05		1.52
5	13	22.86	1.52	3.30
	14	23.62		1.52
	15	27.43		1.27
6	16	29.46		1.27
	17	31.24		3.81
	18	32.26		2.03
	19	35.30	1.52	2.03

The physical and mechanical properties of the shaft and the disk are represented in Table 4.2. The bearings are modelled as linear springs. Two types of bearings are considered for the analysis. First one is isotropic bearing for which the stiffness values of the bearings in Y and Z axes are $K_{VV} = K_{WW} = 4.378e7$ N/m and the second one is orthotropic bearing for which the stiffness values are $K_{VV} = K_{WW} = 3.503e7$ N/m, $K_{VW} = K_{WW} = -8.756e7$ N/m. Isotropic bearings have physical properties such as stiffness same in all directions, whereas orthotropic bearings have physical properties such as stiffness independent in three mutually perpendicular directions [11].

Table 4.2 Physical and mechanical properties of shaft and disk [11]

Notation	Description	Value
ρ	Density	7860 kg/m^3
E	Modulus of elasticity	2.1 x 10^{11} N/m^2
μ_{el}	Element mass per unit length	0.3
Ω	Spin speed	0-30000 rpm
I_d	Diametric inertia of disk	0.0136 kg-m^2
I_p	Polar inertia of disk	0.0020 kg/m^3
$m_{d1} = m_{d2} =$	Disk mass	1.401 kg

The analysis is carried out by considering the following three cases of the rotor bearing system.

Case 1: Undamped rotor bearing system without crack.

Case 2: Damped rotor bearing system without crack.

Case 3: Undamped rotor bearing system with crack.

a.

b.

c.

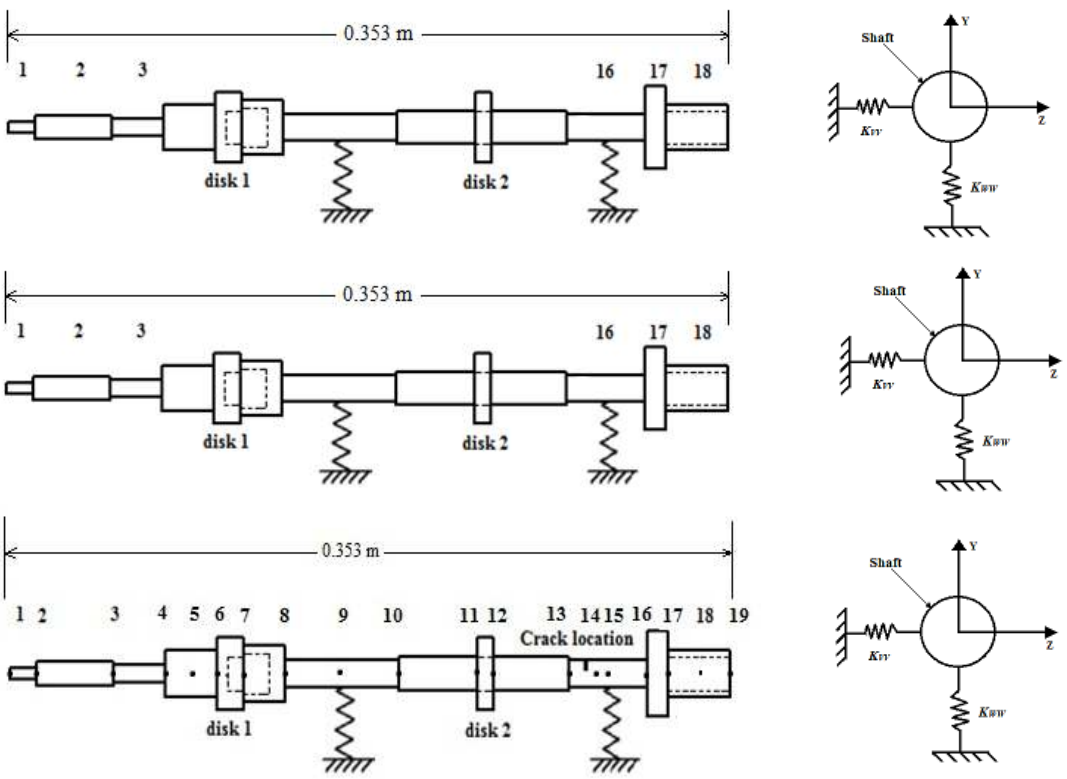

Figure 4.1.1. Finite models of the system (a) Undamped system without crack (b) Damped system without crack, (internal dampings η_H = 0.0002 & η_V = 0.0002s), (c) Undamped system with crack.

4.1 Undamped rotor bearing system without crack

The undamped rotor bearing system without crack is analyzed for natural whirl frequencies, mode shapes, unbalance response and critical speeds. The starting point of the instability regions related to first two forward whirling modes are determined. Two types of bearings i.e. isotropic and orthotropic are considered for the analysis.

4.1.1 Natural whirl frequencies and mode shapes

The natural whirl frequencies for the first three modes of the uncracked rotor bearing system with variable cross sections supported on isotropic and orthotropic bearings for the speed range of 0-30000 rpm in the fixed frame coordinates are found for the 18 elements in first trial. Due to the complexity of the system configuration, convergence study is done with three sets of elements which are 18, 25, and 30 respectively. It is observed that the frequencies of the first three mode shapes are converged with 30 numbers of elements. The convergence results for natural whirl frequencies of isotropic and orthotropic bearings are listed in Table 4.3 and 4.4 respectively.

Table 4.3 Natural whirl frequencies of isotropic bearing.

Modes	Natural whirl frequencies in (Hz) (No. of elements)		
	(18)	(25)	(30)
I	61.70	61.39	61.35
II	247.36	247.18	247.01
III	402.27	402.01	401.9

Table 4.4 Natural whirl frequencies of orthotropic bearing.

Modes	Natural whirl frequencies in (Hz) (No. of elements)					
	(18)		(25)		(30)	
	BW	FW	BW	FW	BW	FW
I	60.78	61.70	60.55	61.5	60.42	61.48
II	241.82	247.36	241.63	247.22	241.45	247.15
III	373.64	402.28	373.38	402.15	373.25	402.04

The first three mode shapes are obtained for spin speed of 0 and 30000 rpm and are represented in the Figs. 4.2 (a), (b) and (c).

a.

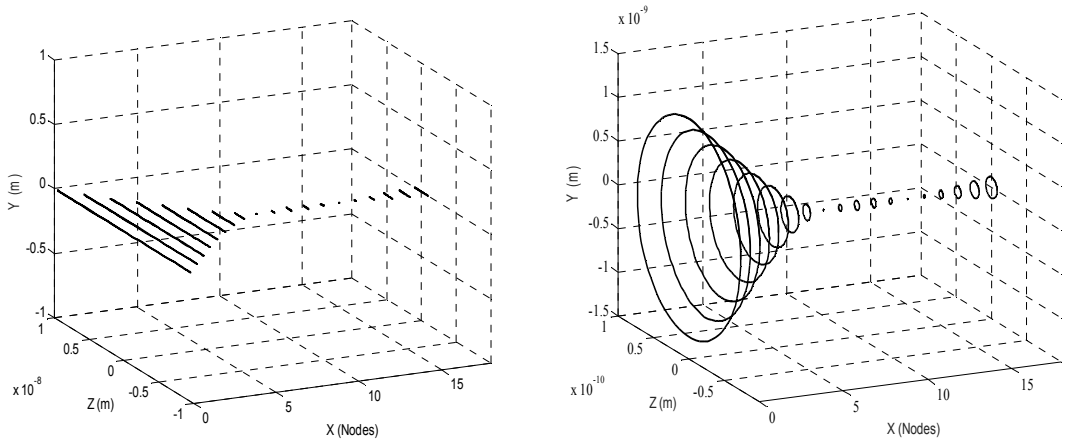

b.

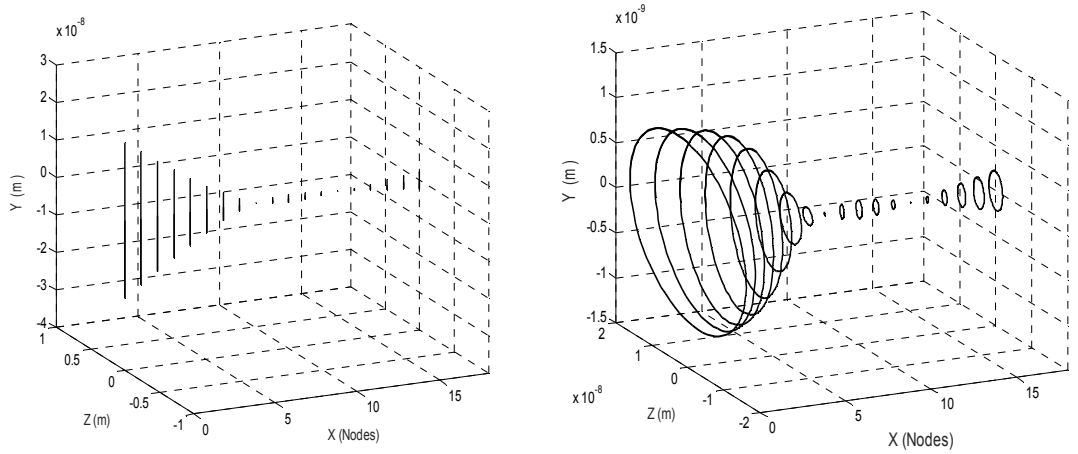

c.

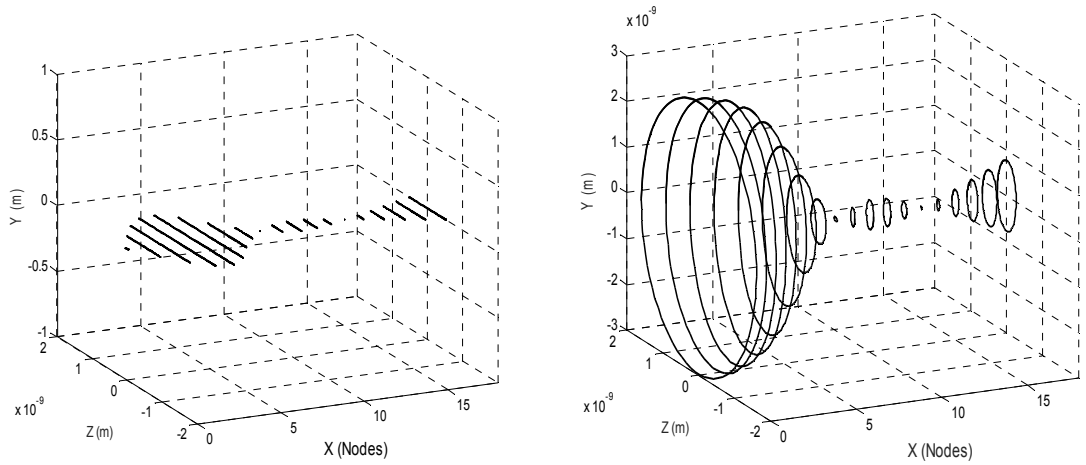

Figure 4.2. Mode shapes at 0 and 30000 rpm (a) First mode shape (b) Second mode shape (c) Third mode shape.

4.1.2 Unbalance response

The element with linear mass unbalance distribution is considered for unbalance response analysis. The disk with mass center eccentricity of 0.001m with (η_L, ζ_L) and (η_R, ζ_R) are calculated and plotted for the two cases of bearing stiffness. The undamped system unbalance response for the fixed frame co-ordinates from the equation (3.52) for the rotor speed range of 0 – 30000 rpm is plotted in Figure 4.3 with isotropic and orthotropic bearings respectively.

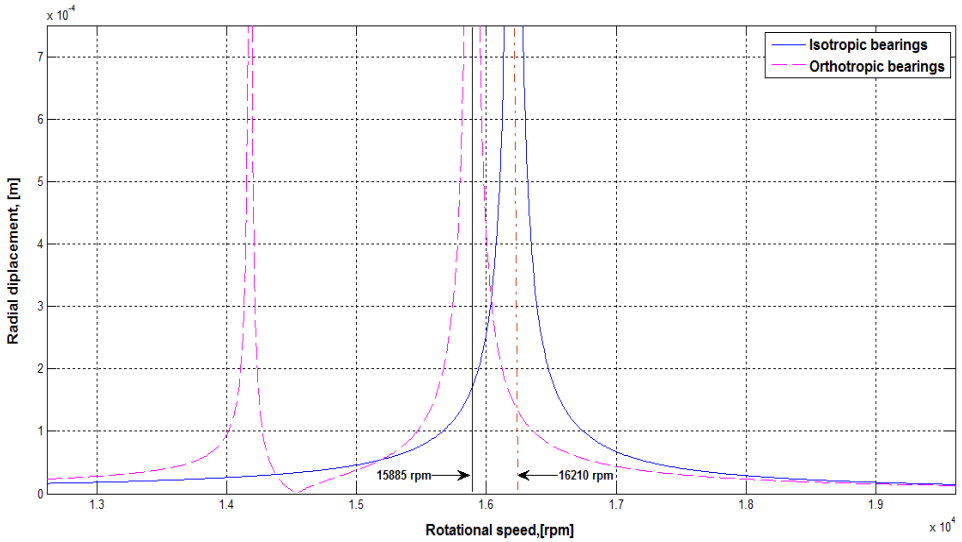

Figure 4.3 Unbalance response of rotor with isotropic and orthotropic bearings

The results are validated with the single disc system [11] for the speed range of 0 – 30000 rpm. The differences for the present study with single and multi disc are listed in the Table 4.5.

Table 4.5 Comparison of critical speeds for isotropic and orthotropic bearings

Types	Speed range (rpm)	Ref. [11] (rpm)	Present work (rpm)	Difference
Isotropic bearing	0 – 30000	1.71 x 10^4	1.688 x 10^4	2.2 %
Orthotropic bearing	0 – 30000	1.65 x 10^4	1.632 x 10^4	1.80%

4.1.3 Natural whirl speeds

The undamped natural whirl speeds associated with the eigenvalue problem of the equation (3.49) for the spin speed of 0-30000 rpm are computed and plotted for the natural whirl ratio of 0, ±1/4, ±1/2 and ±1 in Fig. 4.4 for isotropic and orthotropic bearings respectively.

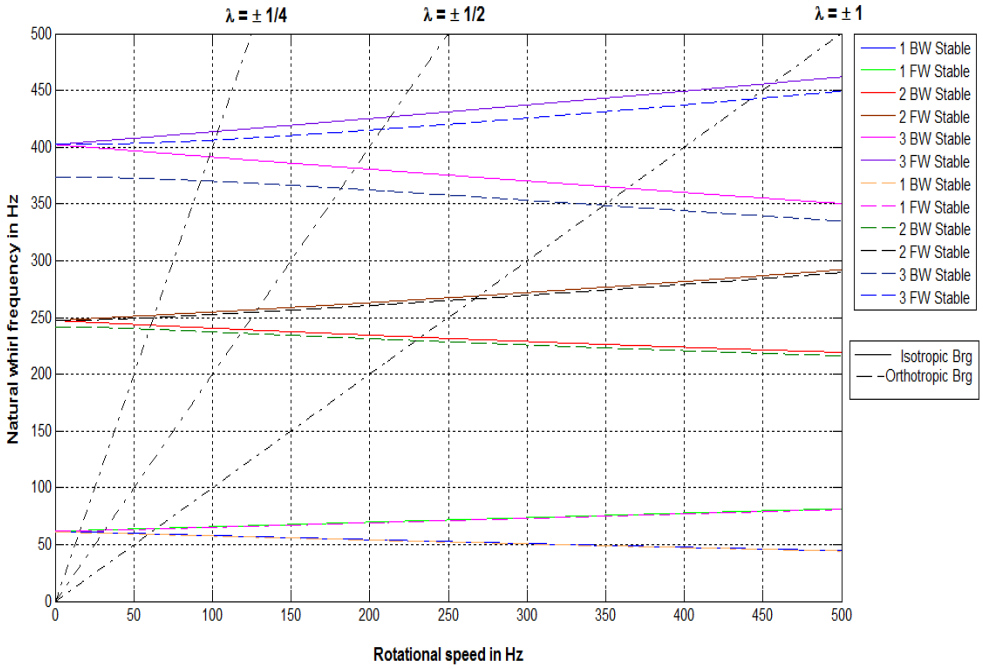

Figure 4.4 Campbell plot for rotor-bearing system with both bearings

The first three natural whirl speeds for each whirl ratio are listed in Table 4.6 for isotropic bearings.

Table 4.6 Natural whirl speeds for isotropic bearing.

Natural whirl ratio	Natural whirl speeds (RPM)	
	Positive	Negative
1	3855	3558
	16164	13974
	27396	21828
1/2	3783	3643
	15456	14358
	25626	22920
1/4	3743	3672
	15126	14610
	24858	23514
0	3702 14841 24136	

The natural whirl speeds of the undamped system by using equation (3.49) for three sets of spin speeds 10000, 20000 and 30000 rpm are obtained for orthotropic bearing. The first three natural whirl speeds for forward and backward cases are presented in table 4.7. It is observed that as the spin speed increases there is an increase in forward speeds and decrease in backward speeds for all modes of vibration.

Table 4.7 Natural whirl speeds for orthotropic bearing.

Spin speed (rpm)	Natural whirl Speeds (rpm)	
	Forward	Backward
10000	4065	3303
	15469	13994
	24707	21902
20000	4416	2962
	16356	13441
	25764	21009
30000	4851	2656
	17371	12970
	26955	20095

4.1.4 System instability regions

The starting points of these instability regions for the periodically time-varying system could be expressed in the spinning (rotating speed) axis by using equation (3.48) related to the first two forward whirl modes. In order to find the system instability regions, the rotating speed lines are plotted which is shown in Fig. 4.5. The initial points of instability regions which are related to the first two forward whirl modes are determined. These instability regions can be given as Ω^p = 3799.8 rpm for PIR and Ω^c = 9690 rpm for CIR.

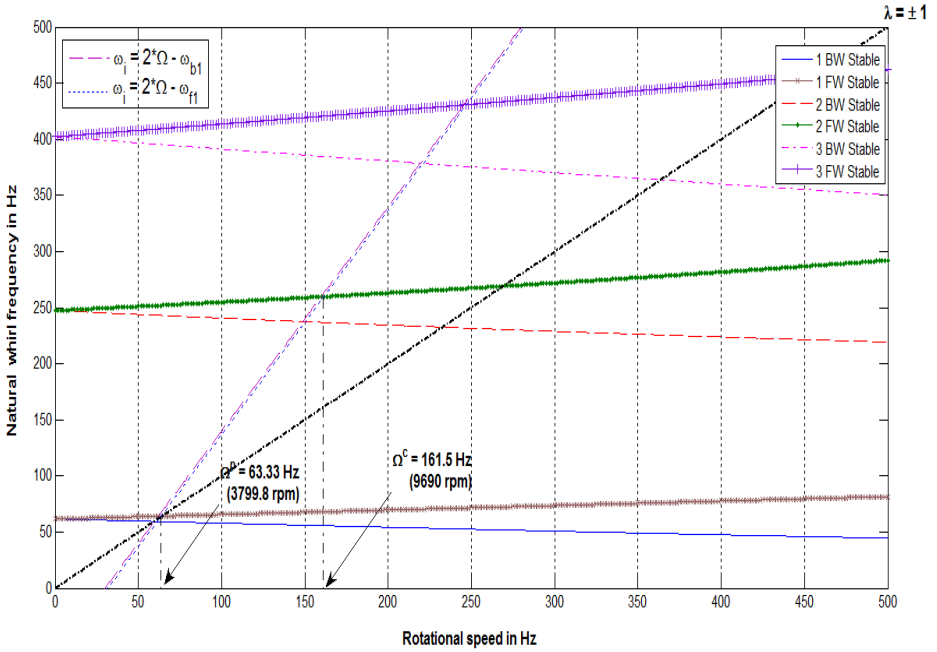

Figure 4.5 The starting points of instability regions related to I and II FW whirl modes

4.2 Damped rotor bearing system without crack

4.2.1 System with hysteretic damping

The multi disk rotor bearing system which is supported on the two identical linear bearings at stations four and six are analyzed with hysteretic damping loss factor $\eta_H = 0.0002$.

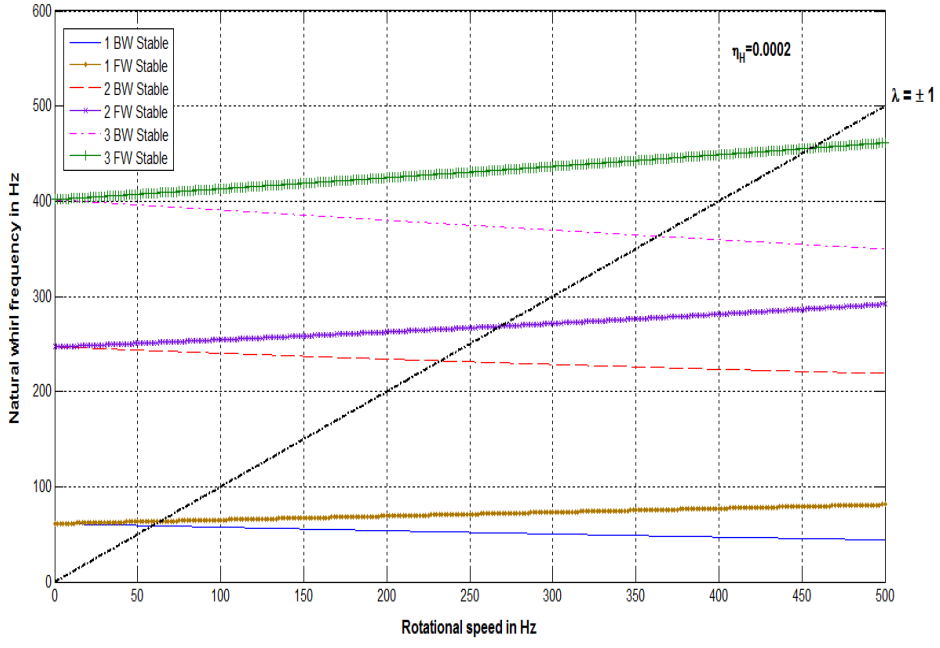

Figure 4.6 Natural whirl frequency of rotor with hysteretic damping on isotropic bearing.

For the synchronous natural whirl, the frequencies of the first three modes are plotted with the speed range of 0 – 30000 rpm for isotropic bearing and shown in Fig. 4.6. Table 4.8 represents the comparison of natural whirl speeds for damped and undamped isotropic bearings for first three modes. From the table it is observed that due to hysteretic damping the natural whirl speed decreases as compared to undamped system.

Table 4.8 Natural whirl speeds for isotropic bearing.

MODES	Damped (rpm) ($\eta_H = 0.0002$)	Undamped (rpm)
I FW	3822	3855
I BW	3536	3558
II FW	16116	16164
II BW	13932	13974
III FW	27360	27396
III BW	21798	21828

Similarly the frequencies of first three modes with hysteretic damping are plotted for orthotropic bearing in Fig. 4.7. The comparison between the hysteric damped and undamped system for orthotropic bearing are represented in Table 4.9.

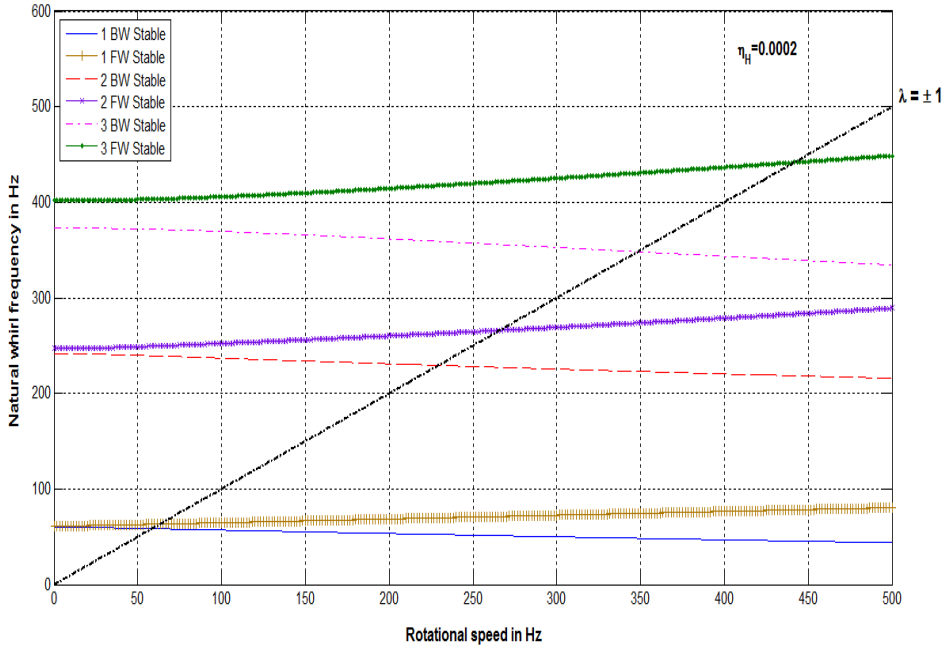

Figure 4.7 Natural whirl frequency of rotor with hysteretic damping on orthotropic bearings.

Table 4.9 Natural whirl speeds for orthotropic bearing

MODES	Damped (rpm) (η_H = 0.0002)	Undamped (rpm)
I FW	3795	3831
I BW	3508	3544
II FW	15966	15990
II BW	13752	13788
III FW	26502	26538
III BW	20898	20922

Figure 4.9 shows the natural whirl frequencies of the uncracked rotor bearing system supported on orthotropic bearing with damping coefficient η_H = 0.0002. Form tables 4.8 and 4.9 it is observed that due to hysteretic damping the natural whirl speed is decreased for both isotropic and orthotropic bearings.

4.2.2 System with viscous damping

The effect of viscous damping with damping coefficient η_V = 0.0002s on natural whirl speeds for isotropic bearing is analysed. From Table 4.10 the first three natural whirl speeds are obtained and is compared with the undamped case. It is observed the frequencies decreased due to the viscous damping in all cases.

Table 4.10 Natural whirl speeds for isotropic bearing

MODES	Damped (rpm) (η_V = 0.0002s)	Undamped (rpm)
I FW	3822	3855
I BW	3536	3558
II FW	22128	16164
II BW	13920	13974
III FW	27486	27396
III BW	21738	21828

Figure 4.8 shows the variation of rotation speeds with first three natural whirl frequencies for isotropic bearing.

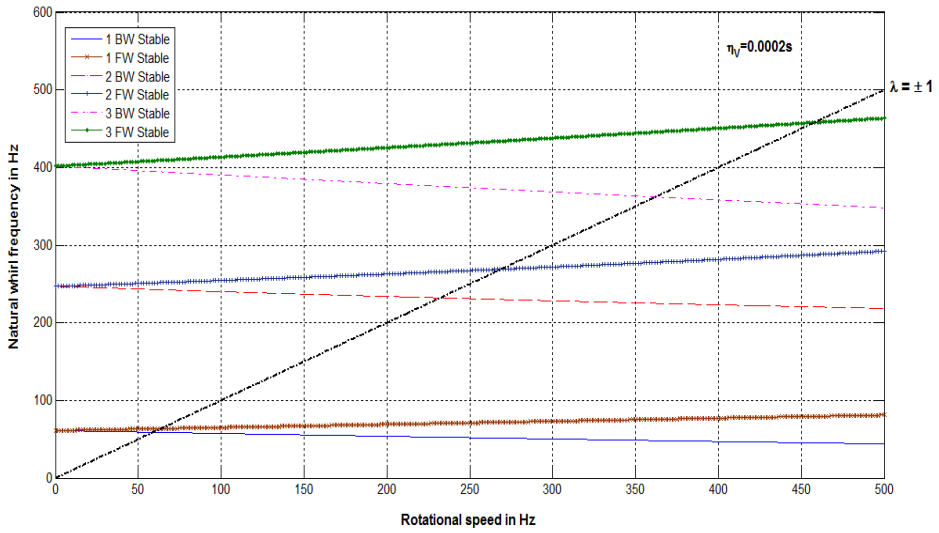

Figure 4.8 Natural whirl frequency of rotor with viscous damping on isotropic bearings.

Similarly for orthotropic bearing the natural whirl frequencies for the first three modes is shown in Table 4.11 and is compared with undamped natural whirl frequencies. The Fig. 4.9 represents the variation of rotational speed with natural whirl frequencies for orthotropic bearing with viscous damping η_V = 0.0002s. From Table 4.10 and 4.11 it is observed that by considering the viscous damping in the system the whirl speed decreased for orthotropic bearing.

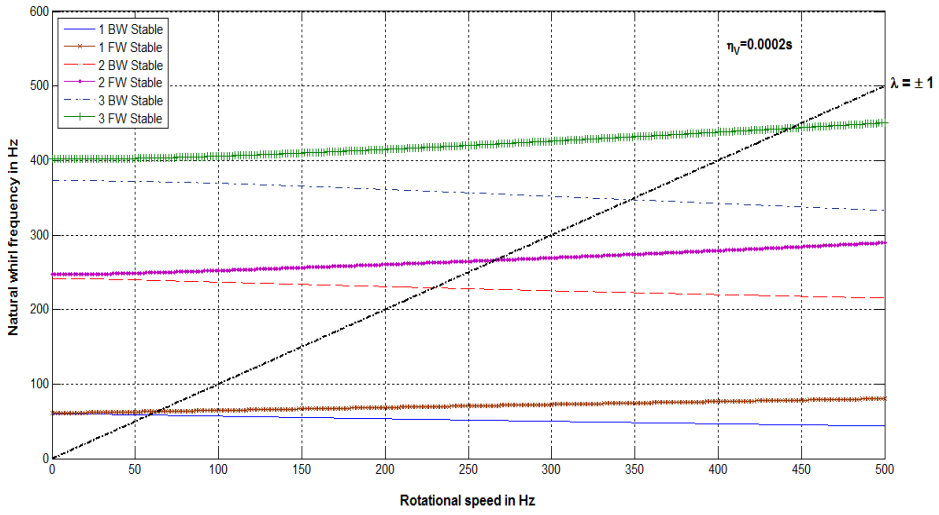

Figure 4.9 Natural whirl frequency of rotor with viscous damping on orthotropic bearings

Table 4.11 Natural whirl speeds for orthotropic bearing.

MODES	Damped (rpm) (η_V = 0.0002s)	Undamped (rpm)
I FW	3795	3831
I BW	3509	3544
II FW	15972	15990
II BW	13752	13788
III FW	26592	26538
III BW	20838	20922

4.3 Undamped rotor bearing system with transverse crack

The undamped rotor bearing system with transverse crack is analyzed for the system shown in Fig 4.10. The transverse crack is assumed to present with relative position of 0.73 and non dimensional crack depth of 0.3. Crack is assumed at an angle of ϕ which is related to the negative fixed Z axis with the time t = 0.

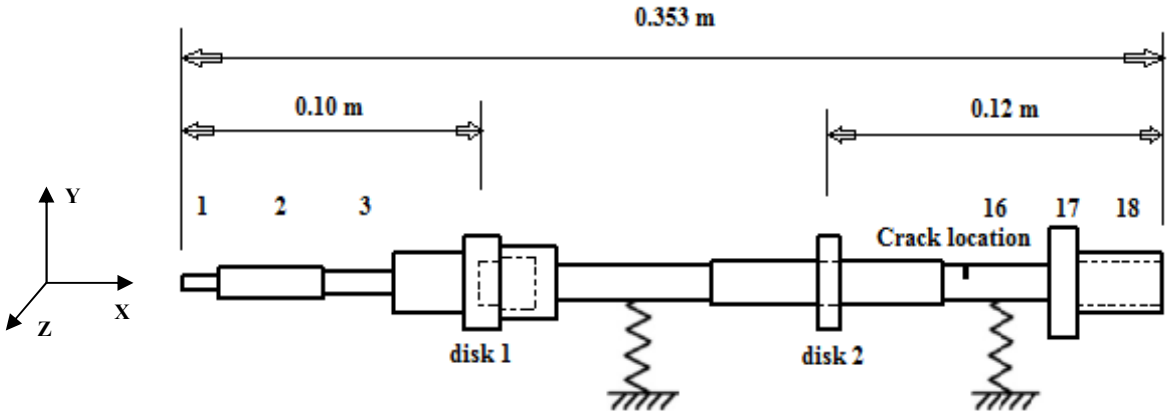

Figure 4.10 Rotor bearing system with variable cross sections and crack

When the rotor shaft rotates the transverse crack angle keep changing with time $\phi + \Omega t$ with respect to the negative Z axis. The system with crack is analysed for the natural whirl frequencies, mode shapes, unbalance response and critical speeds for the time-periodic stiffness matrix with frequency of 2Ω. The starting point of the instability regions, effect of the various non-dimensional crack depth (μ) on the system natural whirl

frequencies, frequency response and phase-plane diagrams are plotted for the system with transverse crack for isotropic bearings and orthotropic bearings.

4.3.1 Natural whirl frequencies and mode shapes

The natural whirl speeds for the first three modes of the cracked rotor bearing system with variable cross sections supported on isotropic and orthotropic bearings for the speed range of 0-30000 rpm in the fixed frame coordinates with the non-dimensional crack depth μ = 0.3 are computed and listed in Tables 4.12 and 4.13 for isotropic and orthotropic bearings respectively for the three sets of spin speeds.

Table 4.12 Natural whirl speeds for isotropic bearing.

Spin speed (rpm)	Natural whirl speeds (rpm)	
	Forward	Backward
10000	3979	3243
	15862	13894
	24734	23265
20000	4366	2919
	16968	13063
	25630	22676
30000	4752	2629
	18096	12316
	26641	22236

Table 4.13 Natural whirl speeds for orthotropic bearing.

Spin speed (rpm)	Natural whirl speeds (rpm)	
	Forward	Backward
10000	3833	3085
	15447	13395
	24661	23190
20000	4204	2779
	16533	12591
	25552	22605
30000	4579	2502
	17712	11862
	26559	22108

The first three mode shapes of the cracked system are computed at the spin speed of 0 and 30000 rpm and are shown in the Figs. 4.11 (a), (b) and (c).

a.

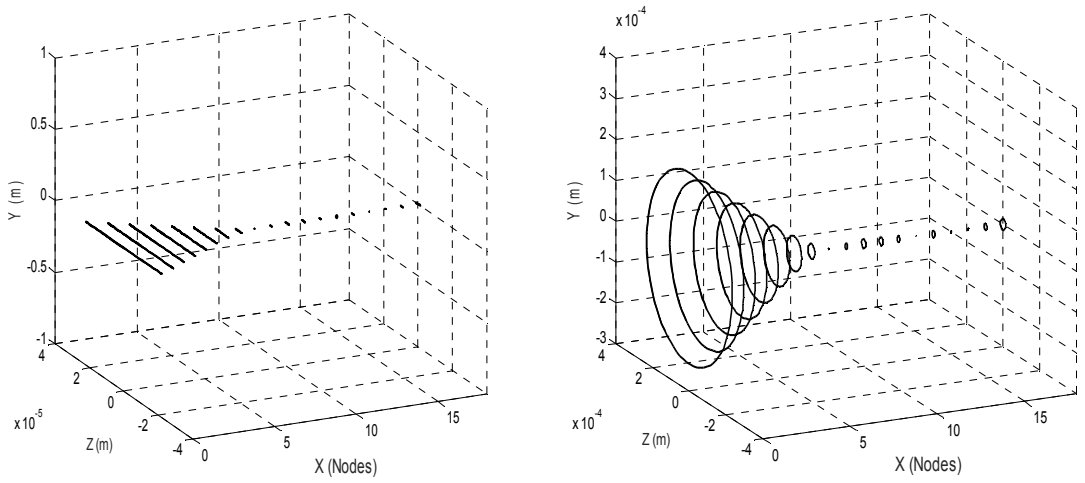

b.

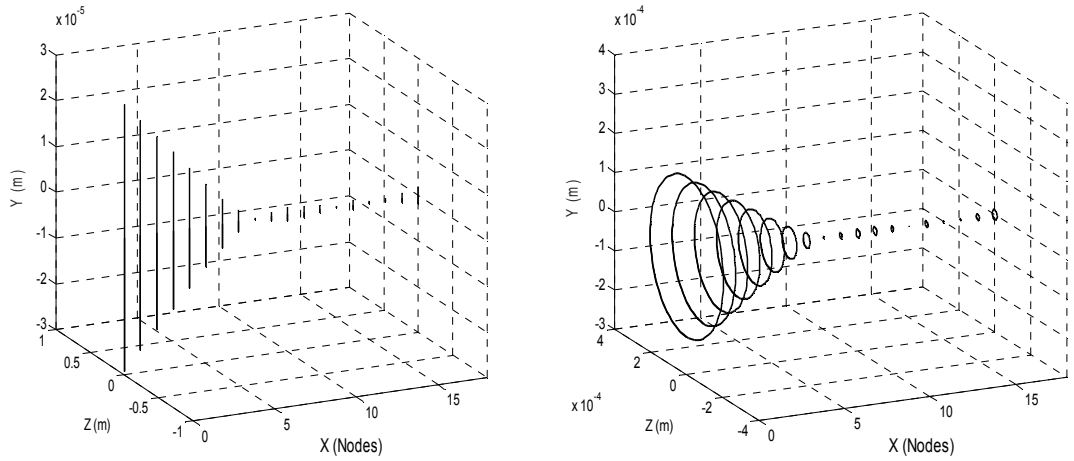

c.

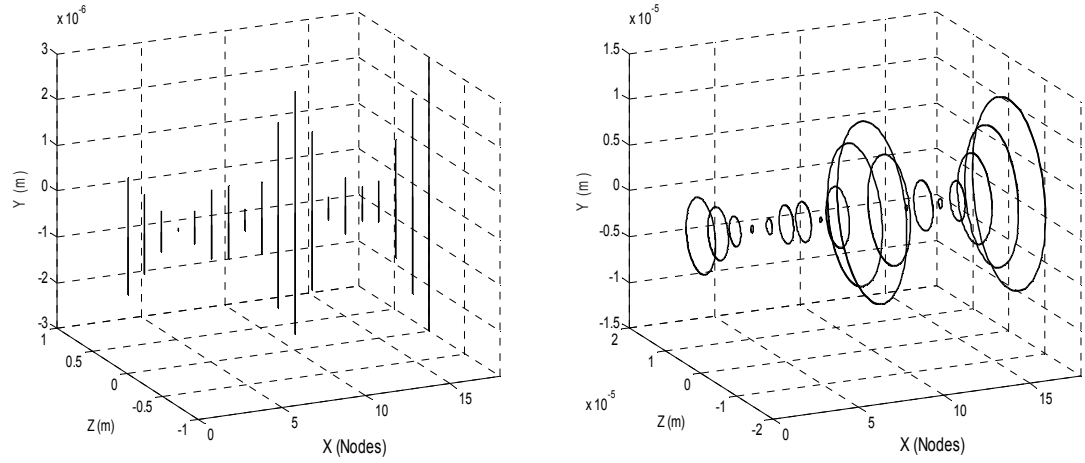

Figure 4.11 Mode shapes for spin speed 0 and 30000 rpm (a) first mode shape (b) second mode shape (c) third mode shape.

4.3.2 Unbalance response with transverse crack

The element with linear mass unbalance distribution is considered for the unbalance response analysis. The disk with mass center eccentricity of 0.001m with (η_L, ζ_L) and (η_R, ζ_R) are calculated and plotted for isotropic and orthotropic bearing stiffness. The unbalance response of the undamped rotor bearing system with a transverse crack in fixed frame co-ordinates from the equation (3.52) for the rotor speed range of 0 – 30000 rpm with the non-dimensional crack depth μ = 0.3 is computed and plotted in Fig. 4.13.

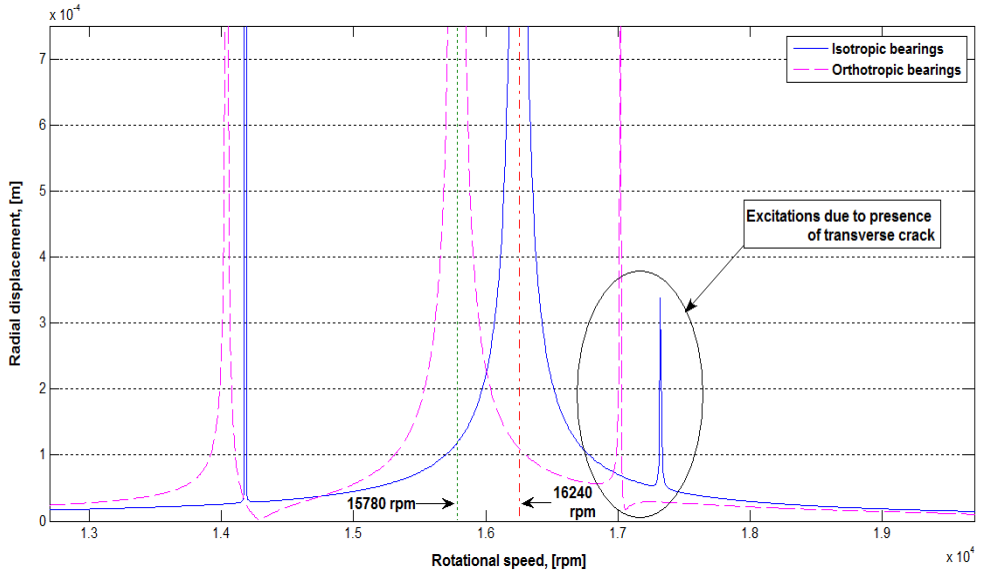

Figure 4.12 Unbalance response of rotor with transverse crack (h/R = 0.3) for isotropic and orthotropic bearings.

4.3.3 System natural whirl speeds with transverse crack

The undamped natural whirl speeds associated with the eigenvalue problem for spin speeds of 0-30000 rpm are computed by using equation (3.49). The variation of rotational speeds with natural whirl frequencies for whirl ratio of 0, ±1/4, ±1/2 and ±1 are shown in Fig. 4.13 for isotropic and orthotropic bearings. The non-dimensional crack depth of 0.3 is considered for the analysis.

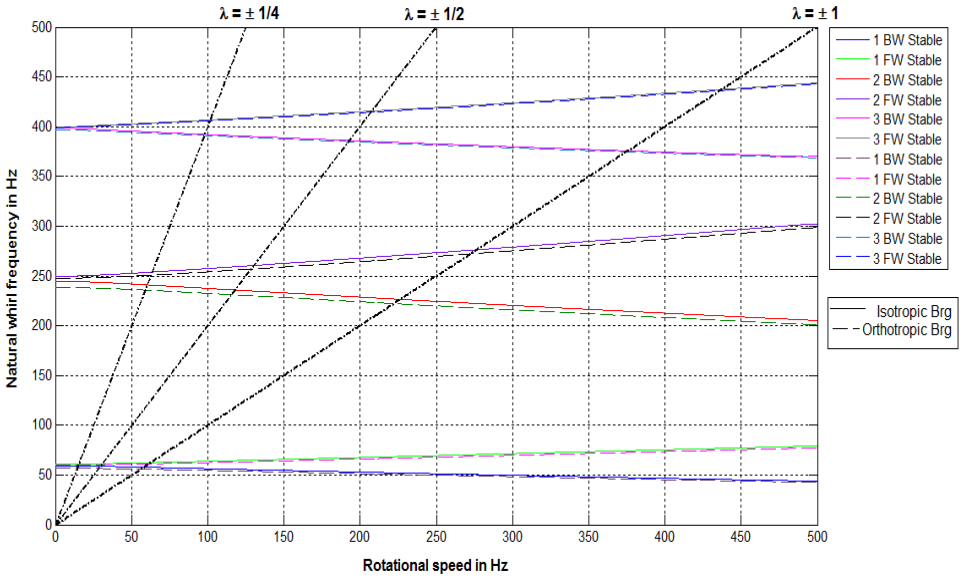

Figure 4.13 Campbell plot for rotor-bearing system with transverse crack for isotropic and orthotropic bearings.

Tables 4.14 and 4.15 represents the natural whirl speeds of the cracked rotor system for the natural whirl ratio of 0, ±1/4, ±1/2 and ±1. It is observed from table that, as the natural whirl speed ratio decreases, there is decrease in whirl speeds.

Table 4.14 Natural whirl speeds for isotropic bearing.

Natural whirl ratio	Natural whirl speeds (rpm)	
	Positive	Negative
1	3742	3470
	16584	13584
	26256	22542
1/2	3679	3530
	15642	14154
	24948	23172
1/4	3647	3554
	15240	14460
	24420	23538
0	3633	3567
	14976	14689
	23950	23945

Table 4.15 Natural whirl speeds for orthotropic bearing.

Natural whirl ratio	Natural whirl speeds (rpm)	
	Positive	Negative
1	3673	3352
	16326	13332
	26190	22482
1/2	3626	3389
	15414	13878
	24882	23106
1/4	3610	3403
	15054	14148
	24354	23466
0	3605	3407
	14859	14304
	23947	23815

4.3.4 Effect of crack depths on natural whirl frequencies

The transverse crack with the asymmetric angle ϕ = 0 for three non-dimensional crack depth, μ = 0.1, 0.2 and 0.3 on the rotor are investigated with the isotropic and orthotropic bearings. The corresponding frequencies for the crack depths for isotropic and orthotropic bearings are shown in Figs. 4.14 and 4.15.

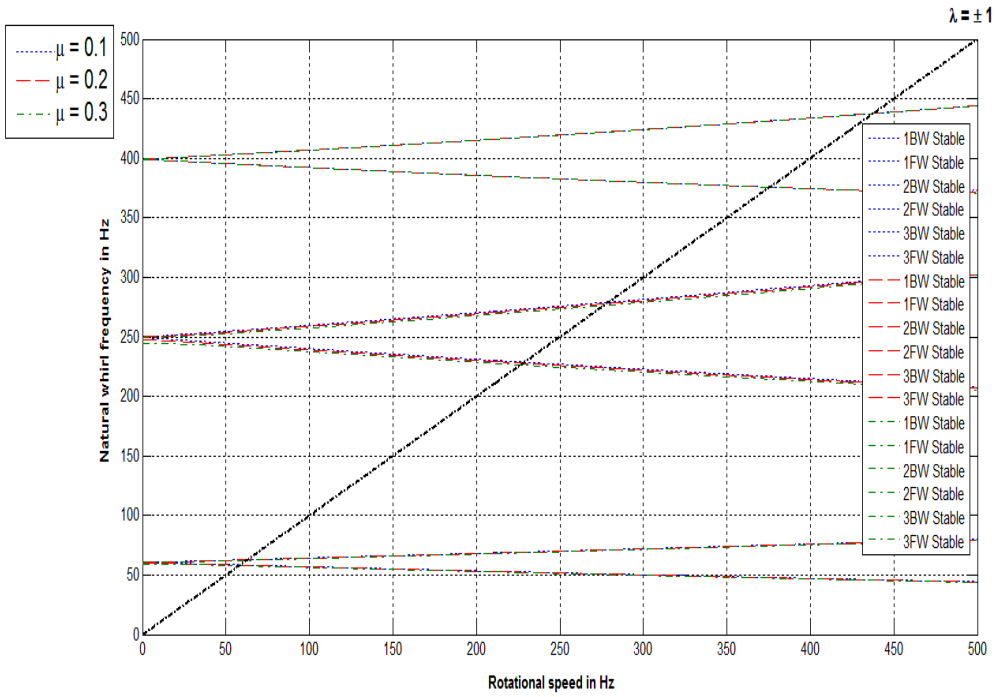

Figure 4.14 Campbell plot for rotor-bearing system with μ = 0.1, 0.2 and 0.3 on natural whirl frequencies for isotropic bearing.

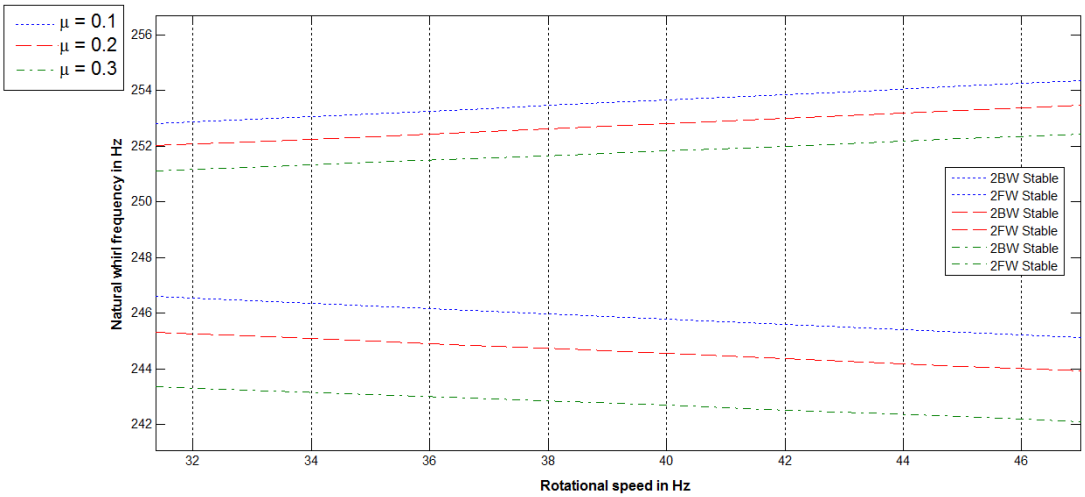

Figure 4.14 (a). Magnified view of II FW and II BW whirls for rotor-bearing system with μ = 0.1, 0.2 and 0.3 on natural whirl frequencies for isotropic bearing.

Similarly for orthotropic bearing the Campbell plot for rotor bearing system of non dimensional crack depths 0.1, 0.2 and 0.3 are plotted in Fig. 4.15.

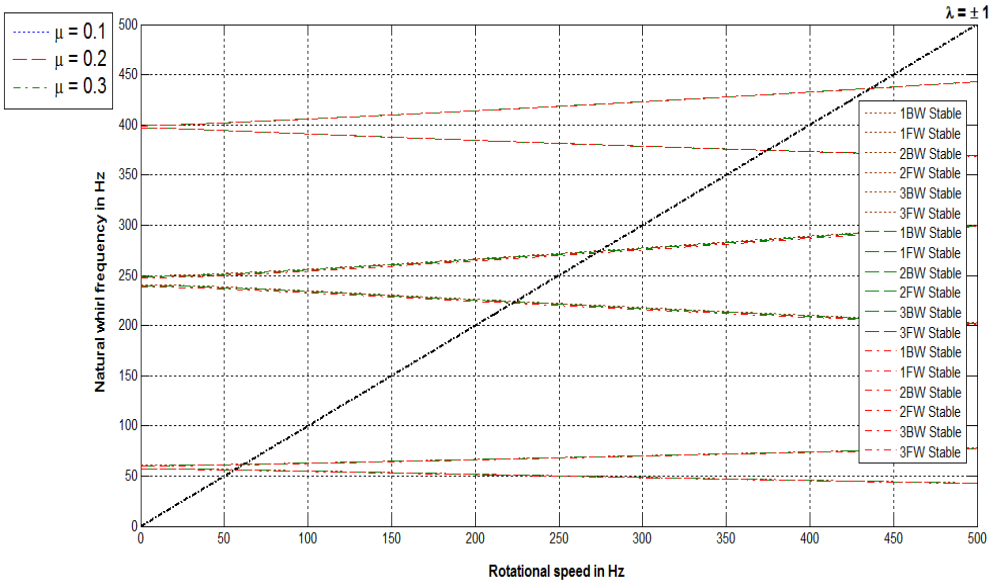

Figure 4.15 Campbell plot for rotor-bearing system with μ = 0.1, 0.2 and 0.3 on natural whirl frequencies for orthotropic bearing.

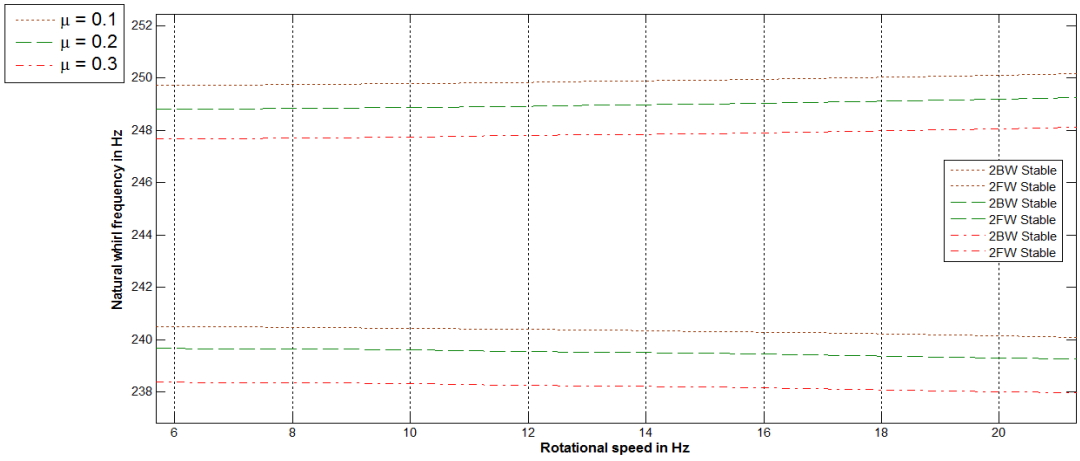

Figure 4.15 (a). Magnified view of II FW and II BW whirls for rotor-bearing system with μ = 0.1, 0.2 and 0.3 on natural whirl frequencies for orthotropic bearing.

Table 4.16 Natural whirl frequencies with μ = 0.1, 0.2 and 0.3 for isotropic bearings.

Modes	Natural whirl Frequency in (Hz)					
	μ = 0.1		μ = 0.2		μ = 0.3	
	FW	BW	FW	BW	FW	BW
I	60.67	60.45	60.63	60.03	60.55	59.45
II	250.18	249.16	249.99	247.28	249.60	244.82
III	399.18	399.16	399.17	399.12	399.17	399.09

Table 4.17 Natural whirl frequencies with μ = 0.1, 0.2 and 0.3 for orthotropic bearings.

Modes	Natural whirl Frequency in (Hz)					
	μ = 0.1		μ = 0.2		μ = 0.3	
	FW	BW	FW	BW	FW	BW
I	60.57	57.35	60.36	57.13	60.08	56.78
II	249.69	240.54	248.77	239.71	247.65	238.41
III	399.17	397.03	399.16	396.99	399.13	396.93

From the Tables 4.16 and 4.17 it is observed that as the crack depth increases there is decrease in natural whirl frequencies for both forward and backward conditions for isotropic and orthotropic bearings. Again for orthotropic bearing the natural whirl frequency is less as compared to isotropic bearing for a given non dimensional crack depth.

4.3.5 System instability regions with transverse crack

For computing the starting points of instability regions related to the first two forward whirl modes equation (3.49) is used. In order to find the system instability regions, the rotating speed lines are plotted which is shown in Fig. 4.16 with non-dimensional crack depth 0.3. These instability regions can be given as Ω^p = 3742 rpm for PIR and Ω^c = 9774 rpm for CIR.

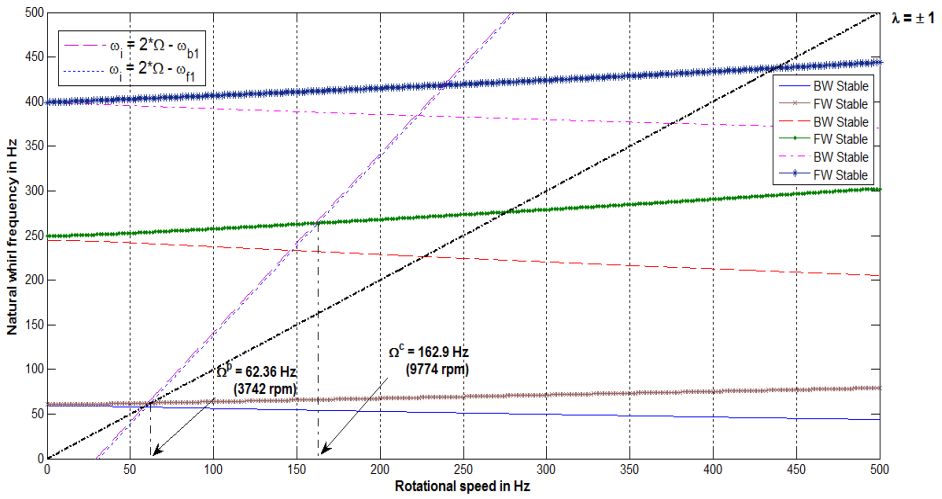

Figure 4.16 The starting points of instability regions related to I and II FW whirl modes with non dimensional crack depth.

4.4 Frequency domain and phase - plane diagrams

The frequency domain and phase – plane diagrams are obtained by using the Houbolt method. This method is an implicit integration scheme, which gives the solutions to coupled second order differential equations. In this, the standard finite difference equations are used to approximate the acceleration and velocity components. This will be in terms of displacement components. This method helps to avoid the critical time step limit, and the time step Δt can be generally used as large as the value given for central difference method [43]. The method utilized here to study the effect of the system spin speed at 1000 rpm and 5000 rpm with disk eccentricity of 0.001m respectively. The responses are analyzed at various nodes in the system.

The following configurations of the systems are analyzed with both the bearing cases to obtain the frequency domain and phase – plane diagrams for the above mentioned parameters,

1. Undamped system without transverse crack
2. Damped system without transverse crack
3. Undamped system with transverse crack

4.4.1 Undamped system without transverse crack

The responses for undamped rotor system with isotropic and orthotropic bearing without transverse crack are shown in Figs. 4.17 - 4.20. The analysis is carried out for spin speeds of 1000 and 5000 rpm with disk eccentricity 0.001m.

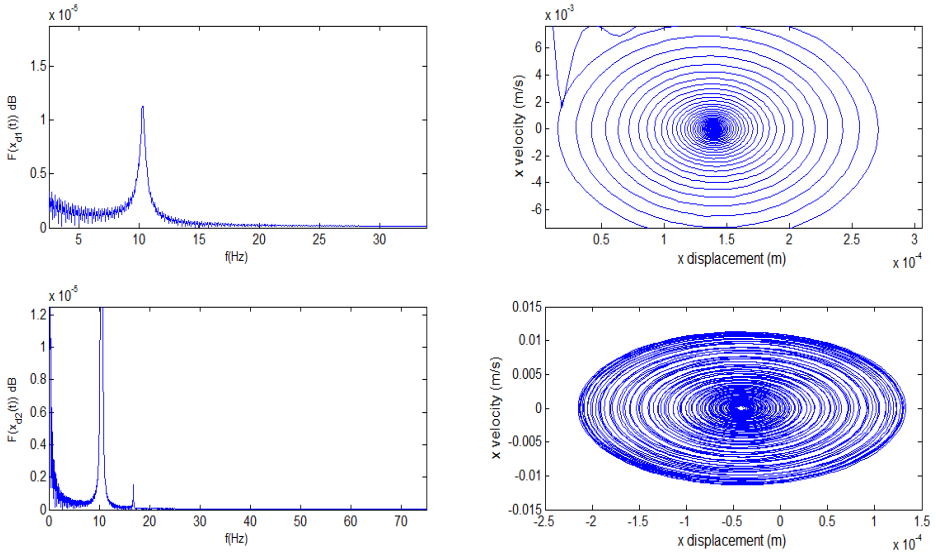

Figure 4.17 Response and phase-plane diagrams of disk 1 and 2 for spin speed 1000 rpm with eccentricity of 1mm for isotropic bearing.

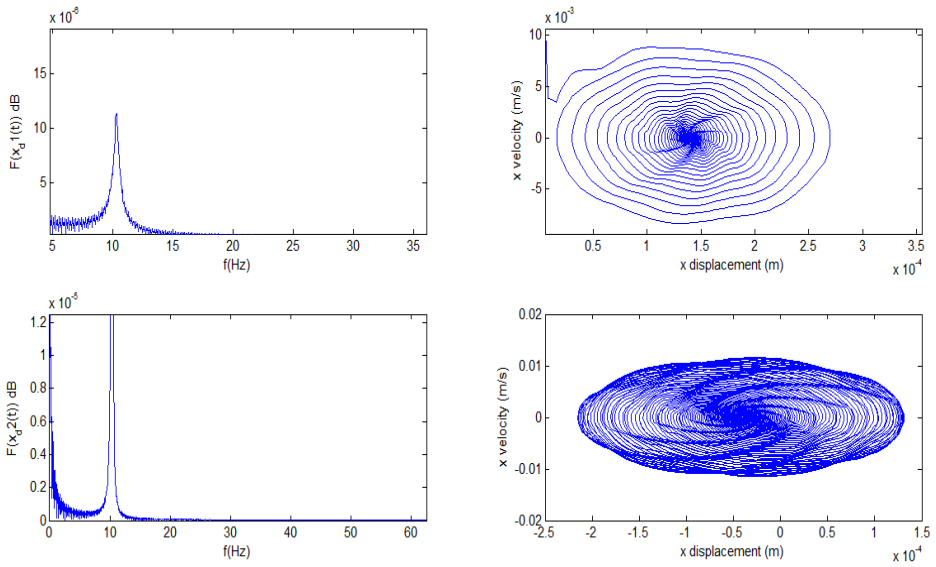

Figure 4.18 Response and phase-plane diagrams of disk 1 and 2 for spin speed 5000 rpm with eccentricity of 1mm for isotropic bearing.

For undamped rotor bearing system without crack at 1000 rpm for isotropic bearing, the amplitude is 1.10e-5 dB for disk-1. Whereas for the same condition, for orthotropic bearing the amplitude is 1.65e-5 dB. The difference in amplitude is due to variation in stiffness of the bearing. When the speed is increased to five times the amplitude for isotropic bearing is 1.13e-5 dB. For orthotropic bearing when the speed increases to 5000rpm, the amplitude is 1.56e-5 dB.

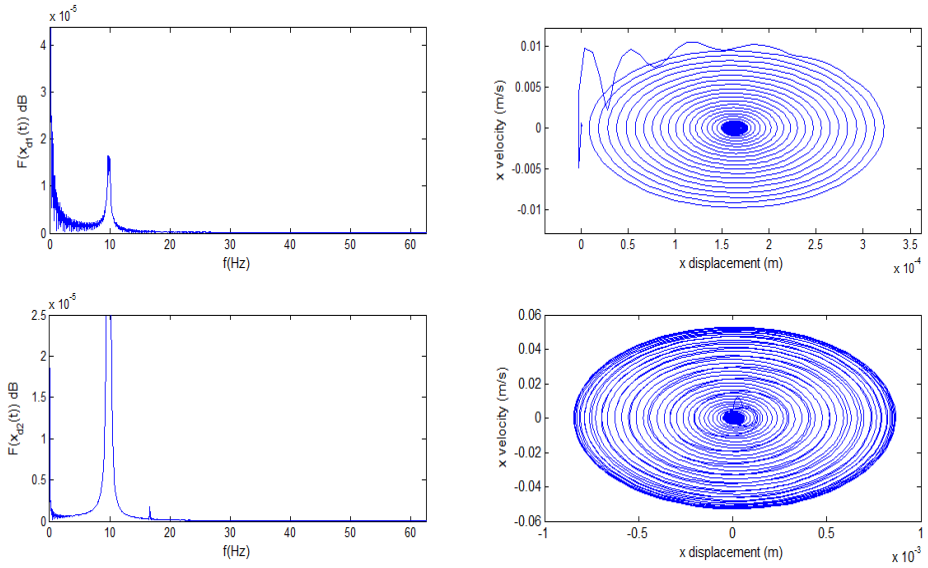

Figure 4.19 Response and phase-plane diagrams of disk 1 and 2 for spin speed 1000 rpm with eccentricity of 1mm for orthotropic bearing.

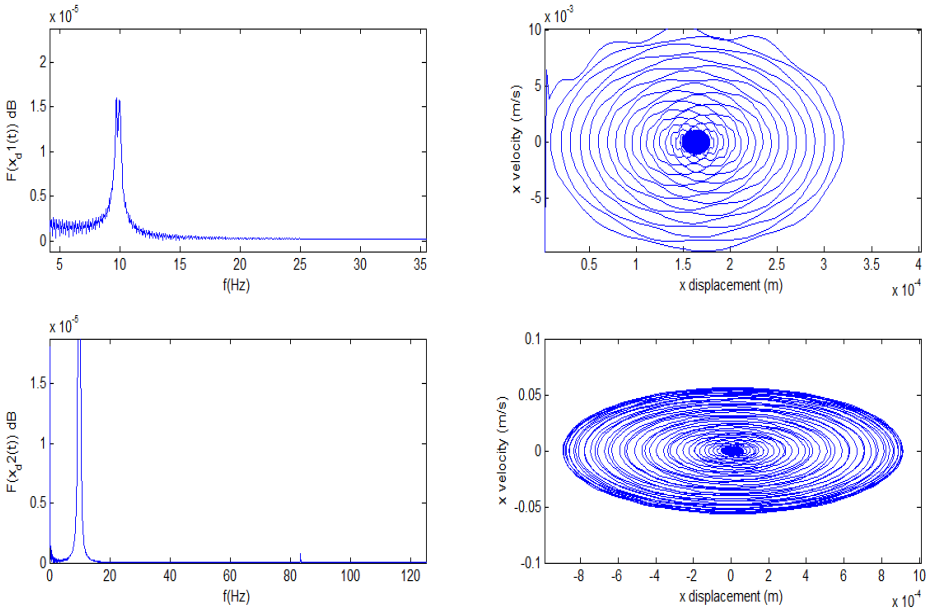

Figure 4.20 Response and phase-plane diagrams of disk 1 and 2 for spin speed 5000 rpm with eccentricity of 1mm for orthotropic bearing.

For disk-2, at 1000rpm for isotropic bearing the amplitude is 6.62e-5 dB. For orthotropic bearing at same speed, the amplitude increased to 19.6e-5 dB. When the speed increases to 5000rpm, the amplitude changes from 6.69e-5 dB for isotropic to 20.45e-5 dB for orthotropic bearing.

4.4.2 Damped system without transverse crack

The effects of damping on frequency response without considering the transverse crack of isotropic and orthotropic bearings are discussed. Two types of dampings are considered for the analysis. First is hysteretic damping where the energy dissipated is independent of frequency of oscillation. Second one is viscous damping in which energy dissipated per cycle depends linearly on frequency of oscillation. The frequency responses along with phase-plane diagrams are shown in Figs. 4.21 – 4.28.

4.4.2.1 Hysteretic Damping without transverse crack

For hysteretic damping the response for frequency with isotropic and orthotropic bearings are shown in Figs. 4.21 – 4.24. Two spin speeds i.e. 1000 rpm and 5000 rpm are considered for the analysis. The disk eccentricity is assumed to be constant as 0.001 m.

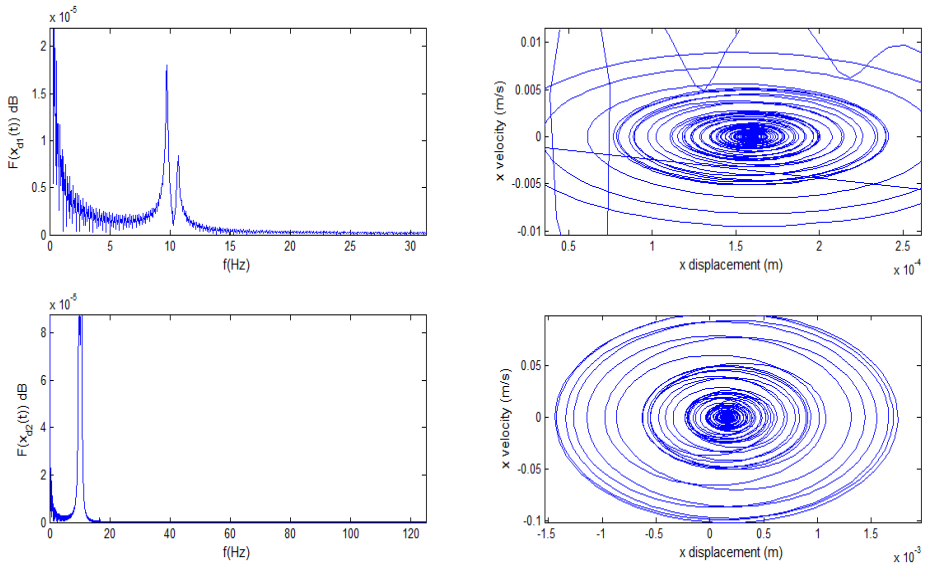

Figure 4.21 Response and phase-plane diagrams of disk 1 and 2 for spin speed 1000 rpm with eccentricity of 1mm for isotropic bearing with hysteretic damping.

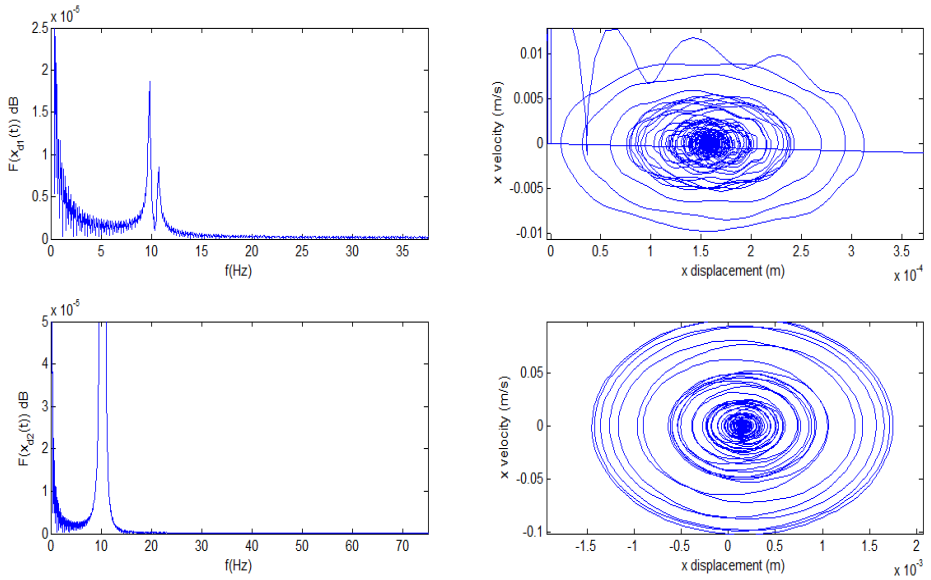

Figure 4.22 Response and phase-plane diagrams of disk 1 and 2 for spin speed 5000 rpm with eccentricity of 1mm for isotropic bearing with hysteretic damping.

For hysteretic damped rotor bearing system without crack at 1000 rpm with isotropic bearing, the amplitude is 1.79e-5 dB. Whereas for orthotropic bearing the amplitude is 2.64e-5 dB at same speed. When speed increased to five times the amplitude for isotropic is 1.86 e-5 dB and that for orthotropic is 2.61e-5 dB for disk-1. Similar characteristics are obtained for isotropic and orthotropic bearings with hysteretic damping for disk-2.

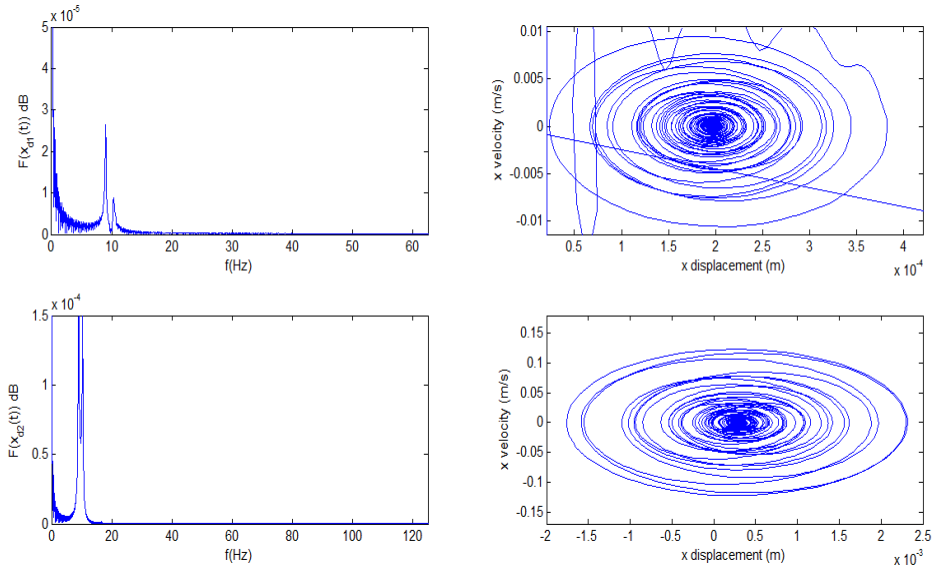

Figure 4.23 Response and phase-plane diagrams of disk 1 and 2 for spin speed 1000 rpm with eccentricity of 1mm for orthotropic bearing with hysteretic damping.

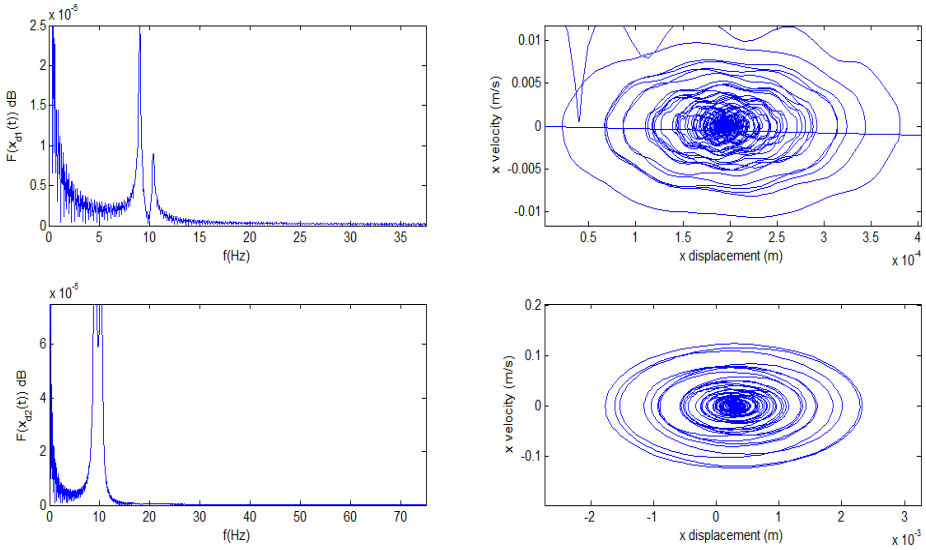

Figure 4.24 Response and phase-plane diagrams of disk 1 and 2 for spin speed 5000 rpm with eccentricity of 1mm for orthotropic bearing with hysteretic damping.

4.4.2.2 Viscous Damping without transverse crack

Figures 4.25 - 4.28 represents the effect of viscous damping on frequency response for isotropic and orthotropic bearings without consideration of transverse crack.

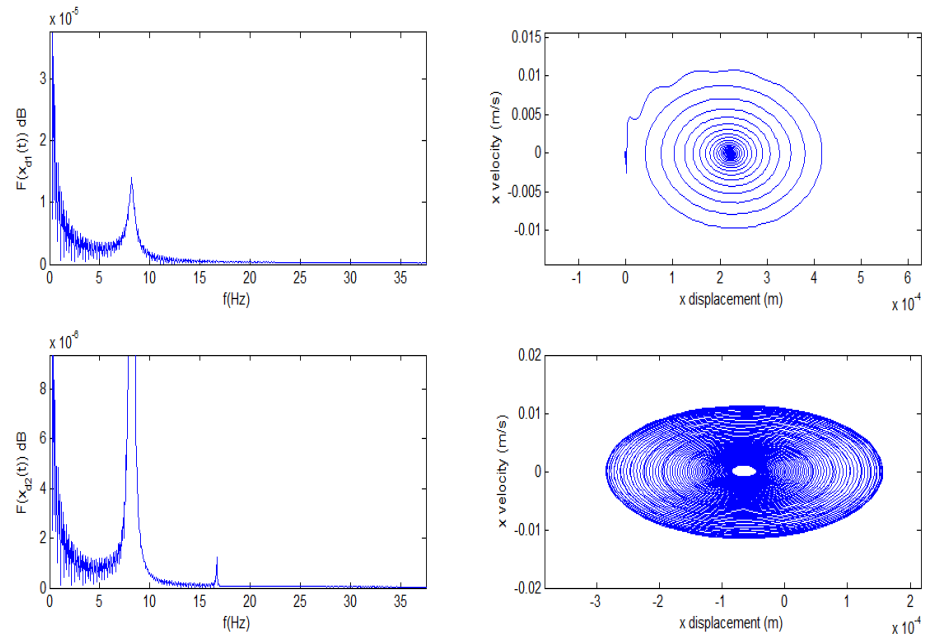

Figure 4.25 Response and phase-plane diagrams of disk 1 and 2 for spin speed 1000 rpm with eccentricity of 1mm for isotropic bearing with viscous damping.

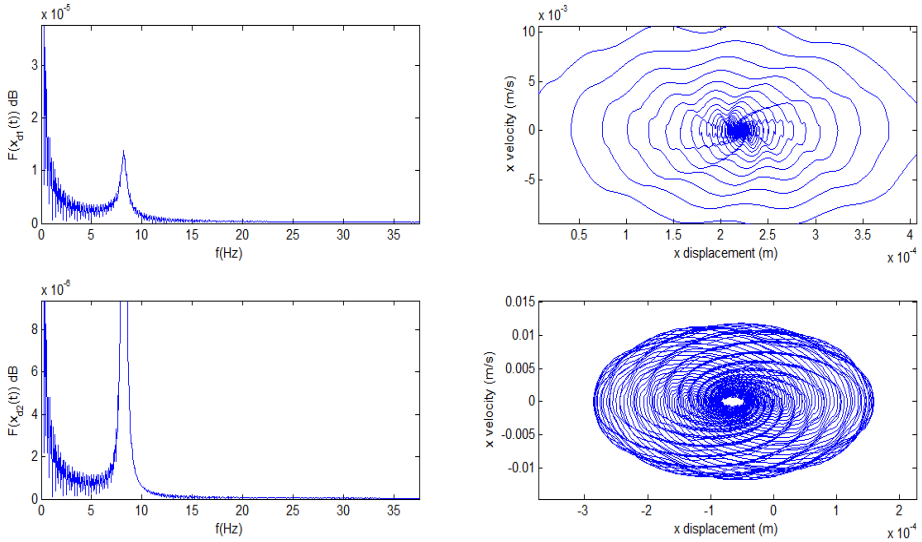

Figure 4.26 Response and phase-plane diagrams of disk 1 and 2 for spin speed 5000 rpm with eccentricity of 1mm for isotropic bearing with viscous damping.

For viscous damped rotor bearing system the amplitude for isotropic bearing is 1.40e-5 dB whereas for orthotropic bearing the amplitude is 3.24e-5 dB for disk-1. When the spin speed increases to 5000 rpm the amplitude is 1.39e-5 dB for isotropic bearing and 3.27e-5 dB for orthotropic bearing. It is observed that the difference in amplitude is negligible when the spin speed increases for both isotropic and orthotropic viscous damping. This is due to very small change in frequency for isotropic and orthotropic bearings.

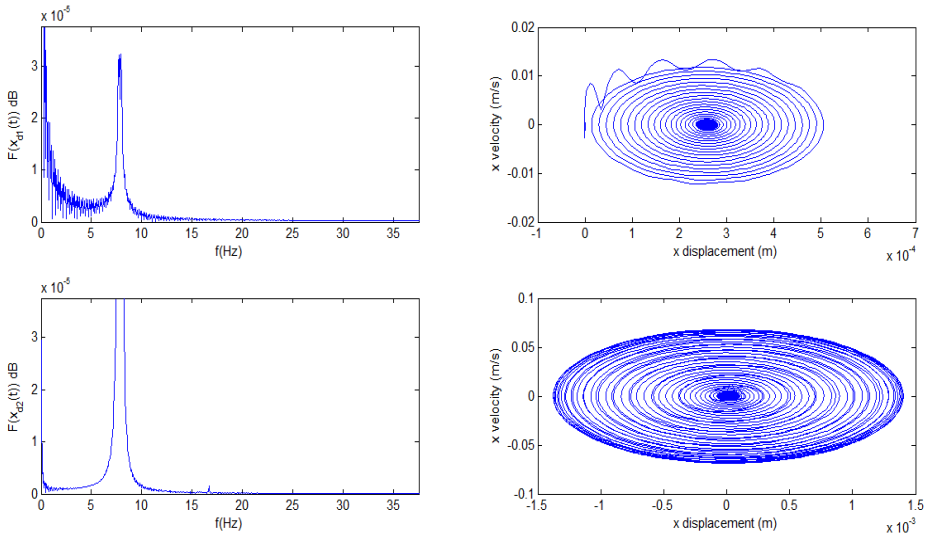

Figure 4.27 Response and phase-plane diagrams of disk 1 and 2 for spin speed 1000 rpm with eccentricity of 1mm for orthotropic bearing with viscous damping.

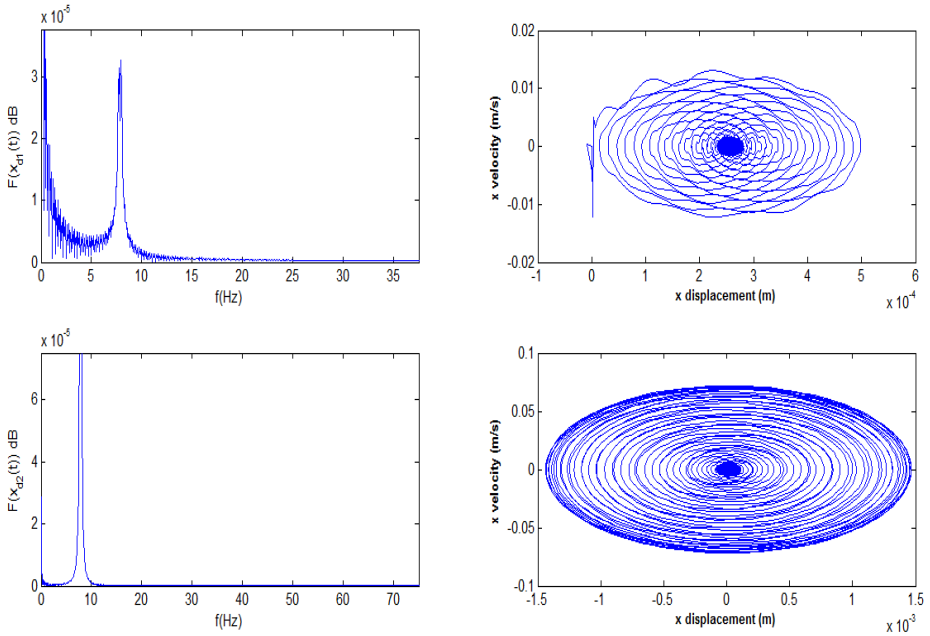

Figure 4.28 Response and phase-plane diagrams of disk 1 and 2 for spin speed 5000 rpm with eccentricity of 1mm for orthotropic bearing with viscous damping.

4.4.3 Undamped system with transverse crack

The responses for undamped rotor system with isotropic and orthotropic bearing with transverse crack are shown in Figs. 4.29 - 4.32. The analysis is carried out for spin speeds of 1000 and 5000 rpm with disk eccentricity 0.001m.

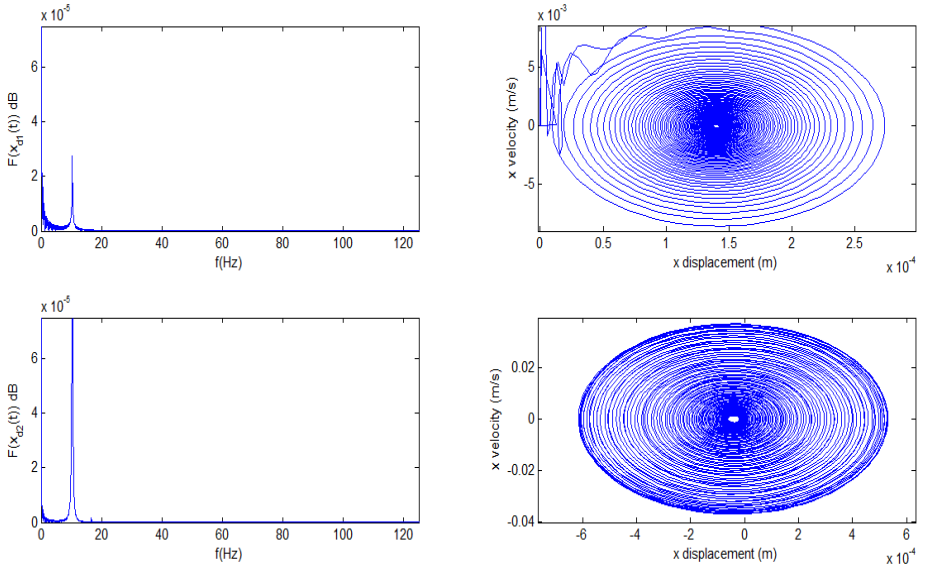

Figure 4.29 Response and phase-plane diagrams of disk 1 and 2 for spin speed 1000 rpm with eccentricity of 1mm for isotropic bearing with transverse crack.

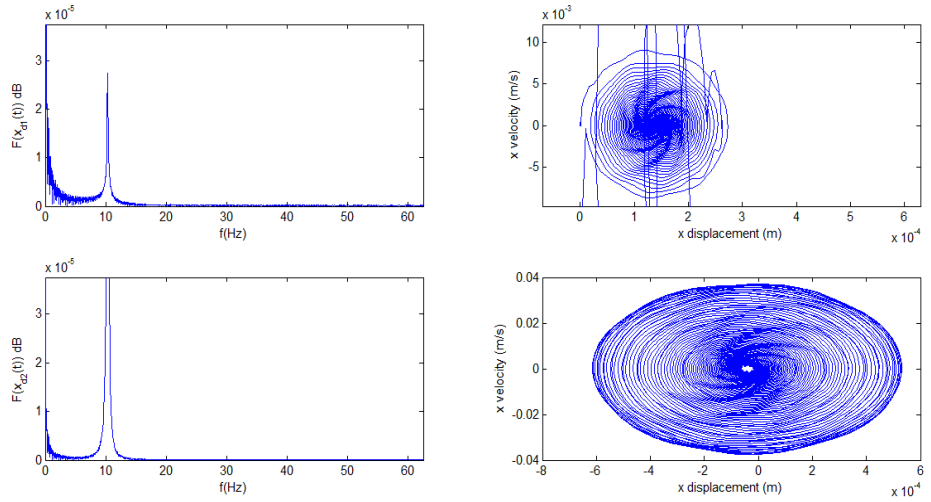

Figure 4.30 Response and phase-plane diagrams of disk 1 and 2 for spin speed 5000 rpm with eccentricity of 1mm for isotropic bearing with transverse crack.

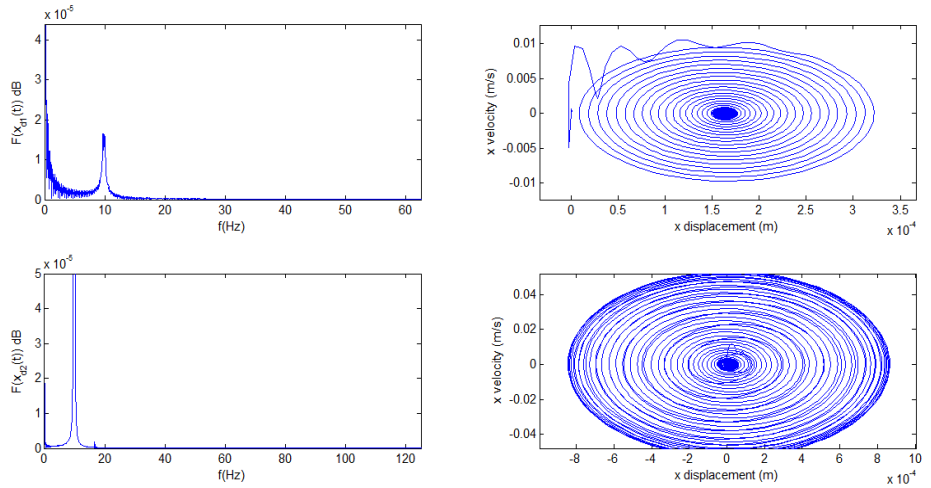

Figure 4.31 Response and phase-plane diagrams of disk 1 and 2 for spin speed 1000 rpm with eccentricity of 1mm for orthotropic bearing with transverse crack.

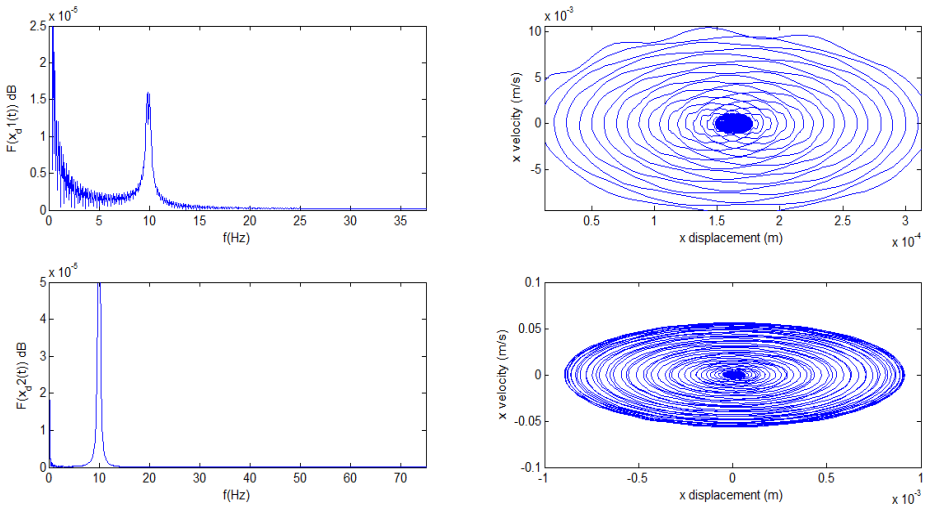

Figure 4.32 Response and phase-plane diagrams of disk 1 and 2 for spin speed 5000 rpm with eccentricity of 1mm for orthotropic bearing with transverse crack.

Similar characteristics are observed for isotropic and orthotropic bearings for undamped cracked rotor (h/R = 0.3, x/L = 0.73) for 1000 and 5000 rpm. For a cracked rotor with isotropic bearings the amplitude is more compared to uncracked rotor. However for orthotropic bearings between cracked and uncracked rotor the change in amplitude is negligible. This is due to very small change in natural frequency between cracked and uncracked rotor.

4.5 Bearing reaction force

The shaft is modelled with SOLID273 axisymmetric elements by using ANSYS® - *v*13 software. The element has quadratic displacement behaviour on the master plane and is well suited for modelling irregular meshes on the master plane. The element has plasticity, hyper elasticity, stress stiffening, large deflection and large strain capabilities. It has also mixed-formulation capability for simulating deformations. The disc is modelled with MASS21 element. This element is defined by a single node, concentrated mass components (f. t^2/L) in the element coordinate directions and rotary inertias (f. L/t^2) about the element coordinate axes.

COMBIN14 is taken for modeling the bearing elements. The element represents a 2-D element and lies in a constant plane. This gives the longitudinal spring-damper option in a uniaxial tension-compression element. The mass for spring-damper element is negligible. Masses are added by using the appropriate mass element.

The system is analysed for transient response for the spin speed range of 0 - 30000 rpm. Bearing reactions for the three time stage period of 0.01 sec with the force of 1 KN is found and plotted in Figure 4.33.

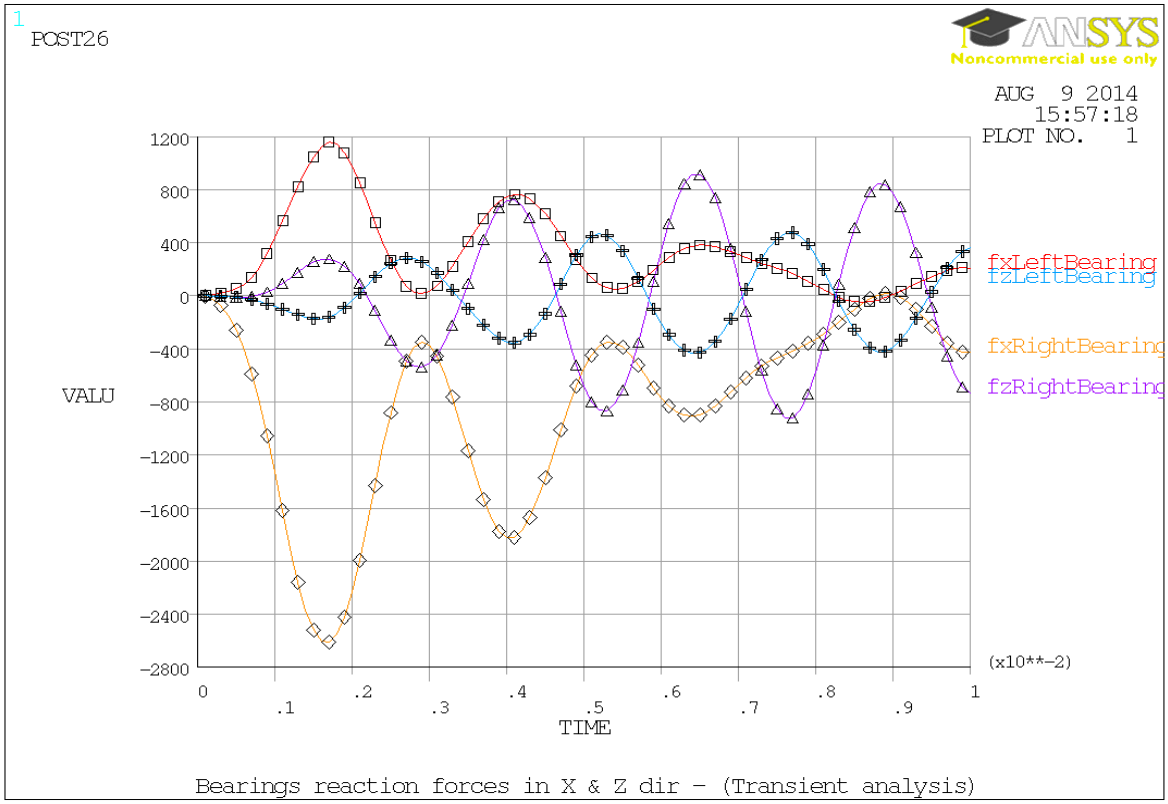

Figure 4.33 Bearing reaction forces – Transient analysis

Figure 4.33 shows the bearing reaction forces performed by transient analysis for the time period of 0.01 sec, which acts in the left and right bearings in both X and Z directions.

4.6. Observations

The flexible multi disk rotor-bearing system is analyzed by finite element method for a typical configuration as shown in Fig. 4.1, which includes a transverse crack and internal damping. The formulation for the crack and internal dampings are made by using finite element method. The analysis carried for three different cases. The effect of crack depths, crack location and rotor speeds are considered as vital parameters in the analysis. As shown in Figs. 4.3 & 4.12, the critical speeds of the rotor-bearing system for the cracked and uncracked system on orthotropic bearings reveals that the critical speed is reduced for the cracked system with increased value of crack depth. The system shows the behavior due to the effect of shaft bending and the time periodic stiffness change. Figs. 4.4 and 4.13 shows the natural whirl frequencies of cracked and uncracked rotor-bearing systems. The natural whirl frequency is less in case of orthotropic bearing due to the fact that they have different stiffness along three mutually perpendicular directions which are independent of each other.

The starting points of the instability regions for the periodically time-varying system are found out and they are shown in Figs. 4.5 and 4.16. It is seen that the starting points of the instability regions are close for the cracked system as compared to the uncracked system. This is due to the whirling speed of the shaft. The frequency response and phase-plane diagrams were carried out by using Houbolt's implicit time integration scheme to study the effect of spin speed with 1000 rpm and 5000 rpm. When the spin speed is increased from 1000 rpm to 5000 rpm the data series in the phase – plane diagrams are disturbed and the frequency domain has a single influenced frequency. The increments of spin speed of the system results in the chaotic motion. The results observed from the finite element approach are compared with the results obtained by Nelson and Vaugh [11] as shown in Table. 4.5. They are found to be in good agreement.

Chapter-5

Conclusions and Future scope

5.1 Conclusions

The present study simulates the dynamics of a multi disk, variable cross section rotor system supported on two bearings at stations four and six, respectively. The theoretical analysis is carried out using FEM approach which offers significant benefits in understanding the dynamic behaviour of rotor-bearing systems. Generally, analysis of higher order sets of equations formulated with finite element approach clearly demonstrates the power of the method and understanding. For the complex rotor system, formulation of the equation of motion, natural whirl frequencies, unbalance response, and the effect of crack depths, crack location and rotor speed are carried for the analysis. The conclusions drawn from the results and discussions are depicted below.

(a) Unbalance response for the uncracked rotor bearing system with variable cross sections supported on isotropic and orthotropic bearings for the spin speed range of 0-30000 rpm has been found, and the results are validated with the single disc system [11] for the same speed range.

(b) The natural whirl frequencies for the first three modes of the uncracked rotor bearing system with variable cross sections were found and the convergence study made with three sets of elements. It is observed that the frequency of the first three modes converges with 30 numbers of elements.

(c) Natural whirl speeds are calculated with the help of 6 station finite element model which includes the 19 sub elements. The forward and the backward whirl modes are obvious due to the gyroscopic effect at all the natural frequencies.

(d) The critical speeds of the system were found with isotropic bearings at 1.621 x 10^4 rpm and orthotropic bearings at 1.5885 x 10^4 rpm respectively. It concludes that, the rotor bearing system should surpass at these critical speeds to avoid the catastrophic failure.

(e) The open crack on the rotor-disk-bearing system seems to have greater impact on the system instability. The instability region frequently raises when the crack depth grows, and the parametric instability swing to fall in minor rotating speed domain.

(f) The starting points of the system instability regions which is related to the first two forward whirl modes for the system without transverse crack were found and given as Ω^p = 3799 rpm and Ω^c = 9690 rpm, and for the system with transverse crack were found and given as Ω^p = 3742 rpm and Ω^c = 9774 rpm.

(g) The analysis of open crack with the asymmetric angle (ϕ=0), the non dimensional crack depth μ and the crack locations on the rotor systems are investigated to show their effects on the system instability regions. The interest rotating speed ranges were found for the PIR (U^p) with speed [3470, 3742] and CIR (U^c) with speed [9660, 9774] rpm.

(h) The frequency response and phase-plane diagrams were carried out by using Houbolt's implicit time integration scheme to study the effect of spin speed with 1000 rpm and 5000 rpm. When the spin speed is increased from 1000 rpm to 5000 rpm the data series in the phase – plane diagrams were disturbed and the frequency domain has a single influenced frequency and the increments of spin speed of the system will result in the chaotic motion.

(i) Transient response analysis was performed for the spin speed range of 0 - 30000 rpm with the help of ANSYS® – *v*13. Bearing reactions for the three time stage period of 0.01 sec with a force of 1 kN was found and plotted in two directions for the left and right bearings.

The frequency response was derived from Houbolt's implicit time integration scheme using an interactive script written in MATLAB® numerical computing software. The frequency response and phase diagrams were obtained at a two specified operating speeds with disc eccentricity of $1x10^{-3}$ m. The presence of transverse crack in the system has a greater impact in the starting point of the system instability regions and when the non-dimensional crack depth 'μ' increases the system natural whirl frequencies falls in the minor rotating speed domain. The results obtained for the rotor system indicates that it can be analysed further with various forms of internal dampings and shear deformation.

5.2 Future scope

The dynamic simulations of a linear system can be analyzed further by incorporating active magnetic bearing (AMB)/fluid film bearings and external dampings into the system configuration. This work can be extrapolated to deal with a non-linear system with the above mentioned systems for the bearing nonlinearities and other factors influenced by the viscous medium. The crack is taken as open in nature here. A breathing crack with time varying function can be used to study the various dynamic behaviour of the system. Multi-disc rotor with disks of asymmetrical inertia and shapes can also be studied. The effects of various disc eccentricities and the operating speeds on the system frequencies and global system vibration response can be properly speculated.

There is a wide scope of analysis on open and breathing transverse cracks for the rotor system. Various effects such as disc eccentricities and operating speeds on the frequencies and overall vibration response can be studied. For the detection of cracks, this can be done inversely with the help of cracked excitation frequencies, crack location and the crack depths by adopting suitable methods.

Bibliography

[1] Genta G. Dynamics of rotating systems. New York: Springer; 2005.

[2] Hong SW, Park JH. Dynamic analysis of multi-stepped, distributed parameter rotor-bearing systems. Journal of Sound and Vibration 1999; 227(4): 769-785.

[3] Joshi BB, Dange YK. Critical speeds of a flexible rotor with combined distributed parameter and lumped mass technique. Journal of Sound and Vibration 1976; 45(3): 441-459.

[4] Lee CW, Jei YG. Modal analysis of continuous rotor-bearing systems. Journal of Sound and Vibration 1988; 126(2): 345-361.

[5] Rao BS, Sekhar AS, Majumdar BC. Analysis of rotors considering distributed bearing stiffness and damping. Computers & Structures 1996; 61(5): 951-955.

[6] Kim YD, Lee CW. Finite element analysis of rotor bearing systems using a modal transformation matrix. Journal of Sound and Vibration 1986; 111(3): 441-456.

[7] Zhao S, Xu H, Meng G, Zhu J. Stability and response analysis of symmetrical single-disk flexible rotor-bearing system. Tribology International 2005; 38: 749–756.

[8] Shih YP, Lee AC. Identification of the unbalance distribution in flexible rotors. International Journel of Mechanical Sciences 1997; 39(7): 841-857.

[9] Tiwari R, Chakravarthy V. Simultaneous identification of residual unbalances and bearing dynamic parameters from impulse responses of rotor–bearing systems. Mechanical Systems and Signal Processing 2006; 20: 1590–1614.

[10] Sinou J.J, Villa C Thouverez F. Experimental and numerical investigations of a flexible rotor on flexible bearing supports. International Journal of Rotating Machinery 2005; 3: 179–189.

[11] Nelson HD, McVaugh JM. The dynamics of rotor-bearing systems using finite elements. Journal of Engineering for Industry 1976; 593-600.

[12] Nelson HD. A finite rotating shaft element using Timoshenko beam theory. Journal of Engineering for Industry 1980; 102: 793-803.

[13] Greenhill LM, Cornejo GA. Critical speeds resulting from unbalance excitation of backward whirl modes. Design Engineering Technical Conferences 3-Part B 1995; 84(2): 991-1000.

[14] Nandi A, Neogy S. An efficient scheme for stability analysis of finite element asymmetric rotor models in a rotating frame. Finite Elements in Analysis and Design 2005; 45: 1343–1364.

[15] Tiwari M, Gupta K, Prakash O. Dynamic response of an unbalanced rotor supported on ball bearings. Journal of Sound and Vibration 2000; 238(5): 757-779.

[16] Sudhakar GNDS, Sekhar A.S. Identification of unbalance in a rotor bearing system. Journal of Sound and Vibration 2011; 330: 2299-2313.

[17] Bachschmid N, Pennacchi P, Vania A. Identification of multiple faults in rotor systems. Journal of Sound and Vibration 2002; 254(2): 327-366.

[18] Sinha JK, Lees AW, Friswell MI. Estimating unbalance and misalignment of a flexible rotating machine from a single run-down. Journal of Sound and Vibration 2004; 272: 967-989.

[19] Arun KJ, Mohanty AR. Model based fault diagnosis of a rotor–bearing system for misalignment and unbalance under steady-state condition. Journal of Sound and Vibration 2009; 327: 604-622.

[20] Vania A, Pennacchi P. Experimental and theoretical application of fault identification measures of accuracy in rotating machine diagnostics. Mechanical Systems and Signal Processing 2004; 18: 329-352.

[21] Pennacchi P, Bachschmid N, Vania A, Zanetta GA, Gregori L. Use of modal representation for the supporting structure in model-based fault identification of large rotating machinery: part 1—theoretical remarks. Mechanical Systems and Signal Processing 2006; 20: 662-681.

[22] Lees AW, Sinha JK, Friswell MI. Model-based identification of rotating machines. Mechanical Systems and Signal Processing 2009; 23: 1884-1893.

[23] Isermann R. Model-based fault-detection and diagnosis – status and applications. Annual Reviews in Control 2005; 29: 71–85.

[24] Xu M, Marangoni RD. Vibration analysis of a motor-flexible coupling-rotor system subject to misalignment and unbalance, part 1: Theoretical model and analysis. Journal of Sound and Vibration 1994; 176(5): 663-679.

[25] Xu M, Marangoni RD. Vibration analysis of a motor-flexible coupling-rotor system subject to misalignment and unbalance, part 2: Experimental validation. Journal of Sound and Vibration 1994; 176(5): 681-691.

[26] Lee CW, Katz R, Ulsoy AG, Scott RA. Model analysis of a distributed parameter rotating shaft. Journal of Sound and Vibration 1988; 122(1): 119-130.

[27] Lee YS, Lee CW. Modelling and vibration analysis of misaligned rotor-ball bearing systems. Journal of Sound and Vibration 1999; 224(1): 17-32.

[28] Sakata K, Kimura K, Park SK, Ohnabe H. Vibration of bladed flexible rotor due to gyroscopic moment. Journal of Sound and Vibration 1989; 131(3): 417-430.

[29] Khulief YA, Mohiuddin MA. On the dynamic analysis of rotors using modal reduction. Finite Elements in Analysis and Design 1997; 26: 41-55.

[30] Ku DM. Finite element analysis of whirl speeds for rotor-bearing systems with internal damping. Mechanical Systems and Signal Processing 1998; 12(5): 599-610.

[31] Chen LW, Ku DM. Dynamic stability analysis of a rotating shaft by the finite element method. Journal of Sound and Vibration 1990; 143(1): 143-151.

[32] Villa C, Sinou JJ, Thouverez F. Stability and vibration analysis of a complex flexible rotor bearing system. Communications in Nonlinear Science and Numerical Simulation 2008; 13: 804–821.

[33] Kalita M, Kakoty SK. Analysis of whirl speeds for rotor-bearing systems supported on fluid film bearings. Mechanical Systems and Signal Processing 2004; 18: 1369-1380.

[34] Genta G. Whirling of unsymmetrical rotors: A finite element approach based on complex co-ordinates. Journal of Sound and Vibration 1988; 124(1): 27-53.

[35] Thomas DL, Wilson JM, Wilson RR. Timoshenko beam finite elements. Journal of Sound and Vibration 1973; 31(3): 315-330.

[36] Adams ML. Non-linear dynamics of flexible multi-bearing rotors. Journal of Sound and Vibration 1980; 71(1): 129-144.

[37] Nandi A. Reduction of finite element equations for a rotor model on non-isotropic spring support in a rotating frame. Finite Elements in Analysis and Design 2004; 40: 935-952.

[38] Murphy BT, Vance JM. An improved method for calculating critical speeds and rotordynamic stability of turbo-machinery. Journal of Engineering for Power 1983; 105: 591-595.

[39] Lee DS, Choi DH. Reduced weight design of a flexible rotor with ball bearing stiffness characteristics varying with rotational speed and load. Journal of Vibration and Acoustics 2000; 122; 203-208.

[40] Wenhui X, Yougang T, Yushu C. Analysis of motion stability of the flexible rotor-bearing system with two unbalanced disks. Journal of Sound and Vibration 2008; 310: 381-393.

[41] Patel TH, Darpe AK. Experimental investigations on vibration response of misaligned rotors. Mechanical Systems and Signal Processing 2009; 23: 2236-2252.

[42] Zorzi ES, Nelson HD. Finite element simulation of rotor bearing systems with internal damping. Journal of Engineering for Power 1977; 99: 71-76.

[43] Rao SS. Mechanical Vibrations. Pearson Asia; 4th edition: 2012.

[44] Papadopoulos CA. The strain energy release approach for modeling cracks in rotors: A state of the art review. Mechanical Systems and Signal Processing 2008; 22: 763-789.

[45] Chasalevris AC, Papadopoulos CA. Coupled horizontal and vertical bending vibrations of a stationary shaft with two cracks. Journal of Sound and Vibration 2008; 309: 507-528.

[46] Dimarogonas AD, Papadopoulos CA. Vibration of a cracked shaft in bending. Journal of Sound and Vibration 1983; 91(4): 583-593.

[47] AL-Shudeifat MA, Butcher EA, Stern CR. General harmonic balance solution of a cracked rotor-bearing-disk system for harmonic and sub-harmonic analysis: Analytical and experimental approach. International Journal of Engineering Science 2010; 48: 921-935.

[48] Chen C, Dai L, Fu Y. Nonlinear response and dynamic stability of a cracked rotor. Communications in Nonlinear Science and Numerical Simulation 2007; 12: 1023-1037.

[49] Darpe AK, Gupta K, Chawla A. Dynamics of a two-crack rotor. Journal of Sound and Vibration 2003; 259(3): 649-675.

[50] Fu YM, Zheng YF. Analysis of non-linear dynamic stability for a rotating shaft-disk with a transverse crack. Journal of Sound and Vibration 2002; 257(4): 713-731.

[51] Gasch R. A survey of the dynamic behaviour of a simple rotating shaft with a transverse crack. Journal of Sound and Vibration 1993; 160(2): 313-332.

[52] Gasch R. Dynamic behaviour of the Laval rotor with a transverse crack. Mechanical Systems and Signal Processing 2008; 22: 790-804.

[53] Sekhar AS. Vibration characteristics of a cracked rotor with two open cracks. Journal of Sound and Vibration 1999; 223(4): 497-512.

[54] Sekhar AS, Dey JK. Effects of cracks on rotor system instability. Mechanism and Machine Theory 2000; 35: 1657-1674.

[55] Sekhar AS. Multiple cracks effects and identification. Mechanical Systems and Signal Processing 2008; 22: 845-878.

[56] Sinou JJ. Effects of a crack on the stability of a non-linear rotor system. International Journal of Non-Linear Mechanics 2007; 42: 959-972.

[57] Tasi TC, Wang YZ. The vibration of a multi-crack rotor. International Journal of Mechanical Science 1997; 39: 1037-1053.

[58] Turhan Ö. A generalized Bolotin's methods for stability limit determination of parametrically excited systems. Journal of Sound and Vibration 1998; 216(5): 851-863.

[59] Darpe AK, Gupta K, Chawla A. Coupled bending, longitudinal and torsional vibrations of a cracked rotor. Journal of Sound and Vibration 2004; 269: 33-60.

[60] Sinou JJ, Lees AW. The influence of cracks in rotating shafts. Journal of Sound and Vibration 2005; 285: 1015-1037.

[61] Jun OS, Eun HJ, Earmme YY, Lee CW. Modelling and vibration analysis of a simple rotor with a breathing crack. Journal of Sound and Vibration 1992; 155(2): 273-290.

[62] Sekhar AS, Prasad PB. Dynamic analysis of a rotor system considering a slant crack in the shaft. Journal of Sound and Vibration 1997; 208(3): 457-474.

[63] Sekhar AS. Model-based identification of two cracks in a rotor system. Mechanical Systems and Signal Processing 2004; 18: 977-983.

[64] Jain JR, Kundra TK. Model based online diagnosis of unbalance and transverse fatigue crack in rotor systems. Mechanics Research Communications 2004; 31: 557–568.

[65] Georgantzinos SK, Anifantis NK. An insight into the breathing mechanism of a crack in a rotating shaft. Journal of Sound and Vibration 2008; 318: 279-295.

[66] Binici B. Vibration of beams with multiple open cracks subjected to axial force. Journal of Sound and Vibration 2005; 287: 277-295.

[67] Sinou JJ. Detection of cracks in rotor based on the 2X and 3X super-harmonic frequency components and the crack–unbalance interactions. Communications in Nonlinear Science and Numerical Simulation 2008; 13: 2024-2040.

[68] Darpe AK, Gupta K, Chawla A. Transient response and breathing behaviour of a cracked Jeffcott rotor. Journal of Sound and Vibration 2004; 272: 207-243.

[69] Papadopoulos CA, Dimarogonas AD. Coupled longitudinal and bending vibrations of a rotating shaft with an open crack. Journal of Sound and Vibration 1987; 117(1): 81-93.

[70] Zheng DY, Fan SC. Vibration and stability of cracked hollow-sectional beams. Journal of Sound and Vibration 2003; 267: 933-954.

[71] Hwang HY, Kim C. Damage detection in structures using a few frequency response measurements. Journal of Sound and Vibration 2004; 270: 1-14.

[72] Zheng DY, Kessissoglou NJ. Free vibration analysis of a cracked beam by finite element method. Journal of Sound and Vibration 2004; 273: 457-475.

[73] Sekhar AS, Prabhu BS. Transient analysis of a cracked rotor passing through critical speed. Journal of Sound and Vibration 1994; 173(3): 415-421.

[74] Abraham ONL, Brandon JA, Cohen AM. Remark on the determination of compliance coefficients at the crack section of a uniform beam with circular cross-section. Journal of Sound and Vibration 1994; 169(4): 570-574.

[75] Gounaris GD, Papadopoulos CA. Crack identification in rotating shafts by coupled response measurements. Engineering Fracture Mechanics 2002; 69: 339–352.

[76] Saavedra PN, Cuitiño LA. Crack detection and vibration behaviour of cracked beams. Computers and Structures 2001; 79: 1451-1459.

[77] Nayfeh AH, Mook DT. Nonlinear oscillations. New York: John Wiley; 1979.

List of Publications

S. Bala Murugan and R.K. Behera, “Analysis of flexible rotor-bearing systems with finite elements”, Proceedings of the International Conference on Structural Engineering and Mechanics (ICSEM-2013), ISBN 978-93-80813-26-4.pp.73.

S. Bala Murugan and R.K. Behera, “Vibration analysis of multi disk twin-spool rotor-bearing systems”, Proceedings of National Symposium on Rotor Dynamics (NSRD-2014) Bangalore, (Feb-2014) pp.22.

S. Bala Murugan and R.K. Behera., “Nonlinear transient analysis of flexible rotor-bearing systems”, Proceedings of International conference on Innovation in Design, Manufacturing and Concurrent Engineering (IDMC-2014) pp.37.